UNIVERSITÉ DU QUÉBEC À MONTRÉAL

GEOCHEMICAL STUDY OF THE CIRCULATION

OF THE GEOTHERMAL FLUIDS OF LOS AZUFRES, MEXICO

THESIS

PRESENTED

AS PARTIAL REQUIREMENT

OF THE MASTERS OF EARTH SCIENCES

BY CAROLYNE PICKLER

MAY 2011

UNIVERSITÉ DU QUÉBEC À MONTRÉAL
Service des bibliothèques

Avertissement

UNIVERSITÉ DU QUÉBEC À MONTRÉAL

ÉTUDE GÉOCHIMIQUE DE LA CIRCULATION DES FLUIDES

GÉOTHERMAUX DE LOS AZUFRES, MEXIQUE

MÉMOIRE

PRÉSENTÉ

COMME EXIGENCE PARTIELLE

DE LA MAÎTRISE EN SCIENCES DE LA TERRE

PAR CAROLYNE PICKLER

MAI 2011

REMERCIEMENTS

TABLE DES MATIÈRES

LISTES DES FIGURES

LISTE DES TABLEAUX

RÉSUMÉ

Une campagne d'échantillonnage de fluides a été effectuée en 2008 et 2009 dans le champ géothermique de Los Azufres, qui se trouve dans la Ceinture Volcanique Transmexicaine, afin de développer de nouveaux outils géochimiques pour tracer l'évolution de ces fluides qui sont exploités pour la production d'énergie électrique. Lors de ces campagnes, une carotte de dépôts hydrothermaux a été prélevée dans le secteur de thermes de Maritaro (Los Azufres) où les phénomènes hydrothermaux à la surface (fumerolles, volcans de boue, etc.) sont les plus actifs. Le but de cette étude était de dater ces évènements hydrothermaux par le moyen des chronomètres ^{226}Ra, ^{228}Ra et ^{210}Pb, en utilisant la méthode développée par Condomines et al. (1999). Pour déterminer les possibles sites minéraux où le radium pourrait se concentrer, la minéralogie et la chimie de la carotte ont été examinées par diffraction des rayons x et par fluorescence des rayons x. Les résultats ont montré la présence de minéraux secondaires comme les argiles (kaolinite) et les sulfates hydratés de potassium (alunite) qui sont des produits d'altération de roches volcaniques par les eaux thermales acides. Les concentrations du radium (^{226}Ra de 0.502 à 1.514 dpm/g, ^{228}Ra de 0.077 à 1.302 dpm/g) et du plomb (^{210}Pb de 0.204 à 0.734 dpm/g) mesurés dans les sédiments montrent une forte diminution par rapport aux teneurs mesurées dans les fluides du champ géothermique de Los Azufres (^{226}Ra de 0.1688 à 3.0989 dpm/g). D'autre part, les ratios ^{228}Ra/^{226}Ra et ^{210}Pb/^{226}Ra s'approchent de l'équilibre séculaire. Cette absence de radium peut être expliquée par l'inhibition de l'adsorption du radium sur les argiles et les sulfates dans un environnent fortement acide avec un pH $\leq$ 3. Néanmoins, en appliquant des modèles chronologiques simples nous pouvons estimer des âges maximaux de 20 à 50 ans de la mise en place des dépôts hydrothermaux superficiels du secteur de Maritaro, démontrant une activité hydrothermale intense.

Mots Clés : radium, dépôts hydrothermale, Los Azufres, Maritaro, fluides hydrothermales

ABSTRACT

In 2008 and 2009, fluids were sampled from the Los Azufres Geothermal Field, Central Mexico, which is located within the Transmexican Volcanic Belt. The aim of the study was to analyze the ^{226}Ra, ^{228}Ra and ^{210}Pb in order to evaluate whether these isotopes could be used to establish a chronology of hydrothermal events, following the methodology developed by Condomines et al. (1999). While sampling, a core of hydrothermal deposits was extracted from the Maritaro hydrothermal deposits. This area features the most active surface hydrothermal activity (fumaroles, mud volcanoes, etc.). To distinguish radium abundance variations due to the occurrence of different preferential radium trapping sites from the radioactive decay of ^{210}Pb, we studied the chemistry and mineralogy of the core using x-ray diffraction and fluorescence. Results showed the occurrence of several secondary minerals such as clays (kaolinite) and sulfates (alunite) which are products of the hydrothermal alteration of siliciclastic sediments and/or volcanic rocks by acidic waters. The analysis of radium and lead (^{226}Ra from 0.502 to 1.514 dpm/g, ^{228}Ra from 0.077 to 1.302 dpm/g, ^{210}Pb from 0.204 to 0.734 dpm/g) showed a strong depletion as compared to the hydrothermal fluids of Los Azufres (^{226}Ra from 0.1688 to 3.0989 dpm/g) and a ^{228}Ra/^{226}Ra and ^{210}Pb/^{226}Ra close to secular equilibrium. The marked absence of radium can be explained by adsorption surfaces on clays and sulfates being inhibited by a strong acidic environment with pH of 3 or less. By applying simple chronological models, we can estimate the maximal age of 20-50 years for the placement of the superficial Maritaro hydrothermal deposits.

Key words: radium, hydrothermal deposits, Los Azufres, Maritaro, hydrothermal fluids

INTRODUCTION GÉNÉRALE

Le ^{210}Pb est un outil chronologique important pour la mesure des taux de sédimentation dans les milieux lacustres et marins et pour les interactions entre le sédiment et l'eau (Appleby et Olfield, 1978; Appleby et al., 1986). Cet isotope peut servir à déterminer une chronologie et des taux d'accumulation de sédiments durant les 100 dernières années. Le ^{210}Pb, radionucléide provenant de la décroissance du ^{238}U, peut être utilisé pour dater des dépôts hydrothermaux (Condomines et al, 2010). Rihs et al. (1997), Condomines et al. (1999) et Rihs et Condomines (2002) ont étudié des dépôts de travertins du Massif Central en France et ont noté des enrichissements importants en ^{226}Ra et ^{228}Ra ($\geq$ 2000 mBq g^{-1}), ces deux isotopes provenant de la décroissance de l'uranium. Il faut noter que durant la précipitation des carbonates, le ^{210}Pb, qui est insoluble, est pratiquement absent dans le système (Rihs et al., 1997). Après le dépôt des carbonates, si le système demeure fermé et le ^{222}Rn est perdu, la détermination du rapport ^{210}Pb/^{226}Ra dépendra seulement de la production *in situ* par décroissance de l'^{238}U. Ces deux isotopes, ^{210}Pb et ^{226}Ra, nous permettent donc de dater ces dépôts sur une échelle temporelle d'un siècle. Le même résultat peut être atteint en utilisant le ^{228}Ra. Le ^{228}Ra décroit en ^{228}Th et la détermination du rapport ^{228}Th/^{228}Ra permet de dater les dépôts jeunes ayant été mis en place entre 0 à 15 ans (Condomines et al., 1999). L'objectif de cette étude est de dater les dépôts hydrothermaux, et à travers eux, d'estimer l'intensité de l'activité thermique d'un champ géothermique. Pour cela une carotte a été prélevée dans les dépôts produits par les sources hydrothermales du secteur Maritaro qui se trouvent dans le champ géothermique de Los Azufres. Le champ géothermique de Los Azufres est le deuxième plus important au Mexique et se trouve dans la partie centrale de la Ceinture Volcanique du Mexique, dans la province de Michoacán (González-Partida et al. 2005). Il s'agit d'un système hydrothermal de haute enthalpie qui est relié à l'activité volcanique ignimbritique de la caldera de Santa Ines (Ferrari et al., 1991).

Le champ géothermique de Los Azufres est divisé en deux secteurs : Maritaro au nord et Tejamaniles au sud. Les sources hydrothermales de Maritaro se trouvent dans une section non-exploitée de la région au nord et sont caractérisées par nombreuses fumerolles et

volcans de boue. Par spectrométrie gamma, la carotte a été analysée pour les teneurs en ^{226}Ra, ^{228}Ra, et ^{210}Pb afin d'utiliser ces nuclides comme chronomètres (Condomines et al., 2010). Nous avons aussi étudié les fluctuations temporelles de ^{228}Ra/^{226}Ra afin de déterminer s'il était possible d'utiliser ces isotopes comme indicateurs d'activité paléo-géothermale, i.e. par la détermination de fluctuations des taux de déposition des sédiments hydrothermaux possiblement reliées aux variations du flux de fluides chauds ramenés à la surface. Étant que les isotopes du radium sont absorbés par des minéraux authigènes, une analyse complète de la minéralogie et de la chimie de la carotte a donc été faite par XRF et XRD. Cela devrait permettre de vérifier si les variations des rapports isotopiques du radium sont liés à la minéralogie/chimie du sédiment ou sont liés aux processus de décroissance.

Les travaux présentés ici font partie d'un projet sur l'étude de la circulation des fluides géothermaux à Los Azufres et sur les variations d'enthalpie liées aux réinjections des fluides exploités. Un aperçu des travaux de terrain qui ont été effectués sur les eaux et les fumerolles du champ de Los Azufres est présenté en Annexe. Les travaux sur la carotte de Maritaro sont présentés sous forme d'un article à soumettre à *Geochemical Journal* à l'été 2011

CHAPITRE I

RADIUM BEHAVIOR IN THE ACIDIC HYDROTHERMAL SPRINGS OF MARITARO, LOS AZUFRES GEOTHERMAL FIELD, MEXICO

Carolyne PICKLER[1], Bassam GHALEB[1], Daniele L. PINTI[1], Alain TREMBLAY[1], Victor-Hugo GARDUNO-MONROY[2]

1   GEOTOP and Département des Sciences de la Terre et de l'Atmosphère, Université du Québec à Montréal, CP 8888 Succ. Centre-Ville, Montréal, QC, H3C 3P8, Canada

2   Universidad Michoacana de San Nicolas de Hidalgo, Instituto de Investigaciones Metalúrgicas, Departamento de Geología y Mineralogía

Abstract.

A core was taken in the hydrothermal deposits of the Maritaro springs, Los Azufres Geothermal Field, Central Mexico. The aim of the study was to analyze the ^{226}Ra, ^{228}Ra and ^{210}Pb in order to evaluate whether these isotopes could be used to establish a chronology of hydrothermal events, following the methodology developed by Condomines et al. (1999). To distinguish radium abundance variations due to the occurrence of different preferential radium trapping sites from the radioactive decay of ^{210}Pb, we studied the chemistry and mineralogy of the core. Results showed the occurrence of several secondary minerals such as clays (kaolinite) and sulfates (alunite) which are products of the hydrothermal alteration of siliciclastic sediments and/or volcanic rocks by acidic waters. The analysis of radium and lead (^{226}Ra from 0.502 to 1.514 dpm/g, ^{228}Ra from 0.077 to 1.302 dpm/g, ^{210}Pb from 0.204 to 0.734 dpm/g) showed a strong depletion as compared to the hydrothermal fluids of Los Azufres (^{226}Ra from 0.1688 to 3.0989 dpm/g) and a ^{228}Ra/^{226}Ra and ^{210}Pb/^{226}Ra close to secular equilibrium. The marked absence of radium can be explained by adsorption surfaces on clays and sulfates being inhibited by a strong acidic environment with pH of 3 or less.

1. Introduction

^{210}Pb is a well-established dating tool used in the study of marine and lacustrine sedimentation and sediment-water interactions (e.g., Appleby and Olfield, 1978; Appleby et al., 1986). It can provide a relative chronology and sedimentation rates of recent sediments as well as information on both vertical and lateral mixing. ^{210}Pb is a radionuclide originating from the decay of the ^{238}U series. The input of ^{210}Pb in aquatic environments occurs mostly from the atmosphere, where ^{210}Pb derives from the decay of parent nuclide ^{222}Rn from soils, whereas in deep marine environments it is derived from the decay of ^{226}Ra contained in the water column. ^{210}Pb in waters is readily adsorbed onto settling sediment particles, which subsequently accumulate on the seafloor. Hence, measured activities of ^{210}Pb in sediments will be higher than those expected by the natural decay of ^{226}Ra in the sediment (the so-called supported-^{210}Pb). The distribution with depth of the excess of ^{210}Pb will be then directly related to the age and settling rate of the sediments.

^{210}Pb can also be used for dating hydrothermal deposits (Condomines et al., 2010). Hydrothermal carbonate deposits from the Massif Central were extremely enriched in highly soluble ^{226}Ra and ^{228}Ra ($\geq$ 2000 mBq g^{-1}; Rihs et al., 1997; Condomines et al., 1999; Rihs and Condomines, 2002). On the other hand, insoluble ^{210}Pb is depleted and is practically absent when carbonates precipitate (Rihs et al., 1997). After deposition, if the system remains closed and ^{222}Rn is lost from the system, the measurement of the disequilibrium ratio ^{210}Pb/^{226}Ra should allow the dating of the deposit on timescales of 100 yrs. Similarly, ^{228}Ra decays into ^{228}Th and the ^{228}Th/^{228}Ra ratio should allow the dating of very young deposits, in the range 0-15 years (Condomines et al., 1999).

On the basis of previous works, we sampled a core in the young hydrothermal deposits of the Marítaro hydrothermal springs located within the Los Azufres Geothermal Field (Mexico; Fig. 1). This field was explored in January 2009 for a complete gas survey of fumaroles, thermal springs and geothermal wells. The core was split into 2 cm sections and each section was analyzed for ^{226}Ra, ^{228}Ra and ^{210}Pb by gamma spectrometry in order to use those nuclides as geochronometers and determine the rate of accumulation of the deposits.

Studying the $^{228}Ra/^{226}Ra$ fluctuations through time we would like to determine whether we could use these isotopes as indicators of "paleogeothermal activity". Because radium isotopes are adsorbed onto authigenic mineral phases, a detailed mineralogical and chemical composition analysis of the core has been also carried out by X-Ray fluorescence and X-ray diffraction. This should allow us to check if radium isotopes and their fluctuations may be related to the mineralogy of the sediment rather than decay processes.

2. Geology of the study area

In January 2009, a ~50 cm long, 3.5 cm diameter core was taken at the Marítaro hydrothermal springs (Fig. 2, Fig. 3). These springs are located within the Los Azufres geothermal field, the second most important geothermal field in Mexico (Pandarinath et al., 2007), located in the central portion of the Mexican Volcanic Belt, which is found in the eastern central part of the state of Michoácan (Fig. 1; González-Partida et al., 2005). The Los Azufres field is a typical high-enthalpy hydrothermal system related to a volcanic caldera collapse and displays intense fracturing (Ferrari et al., 1991). The geothermal field is divided into two distinct regions: Marítaro, in the north, and Tejamaniles, in the south. The Marítaro hydrothermal springs are located in the northern region (Fig. 1). This region is characterized by a single-phase liquid reservoir with an average pressure of 90 bar and average temperature of 300°C (González-Partida et al., 2005). The Marítaro hydrothermal springs lie in a non-exploited region of the Los Azufres geothermal field and contain numerous fumaroles and mud volcanoes.

The geology of the Los Azufres geothermal system can be summarized as follows. The local basement, referred to as the Mil Cumbres andesite, is about 3000 m thick and dated between 18.1 and 5.9 Ma (Arellano et al., 2005). This group of rocks is composed of phenocryst-poor, microlitic andesite, interstratified with rocks of andesitic to basaltic composition, basaltic lava flows, and subordinated dacitic rocks. This unit constitutes the main geothermal reservoir (Verma et al., 2005). The Marítaro hydrothermal springs lie within this region (Fig. 1; Birkle et al., 2001). Silicic volcanism began shortly after the eruption of the last andesites. Three major eruptive centers have been identified: Agua Fría rhyolite, San

Andrés dacite, and Yerbabuena rhyolite. These rhyolites overlie the Mil Cumbres andesite and are frequently fractured, allowing the fluids to reach the surface (Verma et al., 2005).

3. Analytical Methods

3.1 Core Description and Preparation

A 50 cm long, ~3.5 cm diameter PVC tube was plunged into the ground at the previously shown location of the Marítaro hydrothermal springs (Figs. 2, 3). A visual examination of the core allowed us to distinguish several color-distinct zones (Fig. 4). There are two zones of white deposits interpreted to be authigenic deposits. These zones are located at a depth of ~13.5 cm to 16 cm and 19.5 cm to 23 cm from the top. Another zone containing some of these deposits is found from about 15 cm to 19.5 cm. Unlike the other two zones, this section contains several pebbles of less than 0.5 mm diameter. These detrital rock fragments reappear further down the core. A large lithic fragment was found from 26 cm to 29 cm. From ~29 cm to 39 cm, there is a lighter grey homogeneous zone. This zone contains small amounts of the white deposits observed upward. As previously stated, the bottom of the core contains several rocky zones, which are rather homogeneous. A dark grey rocky zone occurs from 39 to 47 cm. The bottom of core is finished with a ~3cm thick brownish grey zone.

In the laboratory, the core was cut along its length using an electric saw. A fishing line was passed through the cut core to split the sediment core in two halves (Fig. 4). The core was sampled every two centimeters for chemistry, mineralogical content and Ra isotope determination. During sampling of one half of the core, we attempted to only remove sediment from its center to limit contamination. Each sample was put into a beaker and left to dry at ambient air for at least 24 hours. The sampled sediments were then reduced into powders with a mortar and pestle, and weighted.

3.2 Gamma Spectrometry

Gamma spectroscopy consists of the measure of the energy of gamma rays emitted by radioactive substances and is used for the measurement of environmental radionuclides such as ^{137}Cs and ^{210}Pb, which can be used for dating or determining sedimentation rates (Adams and Gasparini, 1970; Appleby et al., 1986). The crushed sediment samples were put into vials fitted for the gamma-ray spectrometer. These vials can contain up to 8 g of sediment. The samples were left in the vials for at least 20 days to ensure the complete re-equilibration between ^{226}Ra and the short-lived daughters of the ^{238}U series and equilibration between ^{228}Ra and its daughter ^{228}Ac within the ^{232}Th series (Zielinski and Budahn, 1998). The vials were put into a high-precision Germanium gamma-ray spectrometer (ORTEC® DSPEC jr. 2.0) at the Université du Québec à Montréal. Counting time was fixed at 3 to 4 days to provide adequate counts for the peaks of interest. Ionization, the key process by which a gamma-ray is detected, occurs within the spectrometer. This is where it gives up part or all of its energy to an electron. These now ionized electrons collide with other atoms and liberate more electrons. These liberated charges are directly collected (Adams and Gasparini, 1970). Their energy is measured and recorded by Ortec's Gamma Vision program as peaks in counts per minute. The software takes into account the background noise of the detector and corrects the results.

In this study, measurements were focused on the energy peaks of 6 isotopes: ^{210}Pb (46 keV), ^{212}Pb (238 keV), ^{214}Pb (295 keV, 352 keV), ^{208}Tl (583 keV), ^{214}Bi (609 keV), and ^{228}Ac (338 keV, 911 keV). These isotopes were chosen as they are part of the decay chains of ^{238}U and ^{232}Th (Fig.5a,b), which comprise ^{224}Ra, ^{226}Ra, and ^{228}Ra (Schmidt and Cochran, 2009). Since it is believed that equilibration has been reached in both decay series and due to the short half-lives between the isotopes being measured and the radium isotopes of interest, we can use the measured isotopes to determine the activity of ^{224}Ra, ^{226}Ra, and ^{228}Ra. ^{226}Ra can be determined using 3 different measured peaks: the 295 keV peak of ^{214}Pb, the 352 keV peak of ^{214}Pb, and the 609 keV peak of ^{214}Bi. ^{228}Ra can be measured through the two measured peaks of ^{228}Ac: 338 keV and 911 keV. The 583 keV peak of ^{208}Tl and the 239 keV peak of ^{212}Pb can be used to determine the ^{224}Ra activity (Herranz et al., 2006). While three different peaks were measured and could be used to calculate the activity of ^{226}Ra, only the

peak of ^{214}Pb at 352 keV was used. It is better to use this peak rather than that of ^{214}Bi because corrections for the cascade-summing effect must be relied on to correctly determine the ^{214}Bi peak. The 352 keV peak of ^{214}Pb is chosen over that at 295 keV due to its greater photon emission probability, 37.6% compared to 18.2% (Herranz et al., 2006). For ^{224}Ra, we chose to calculate its activity using the ^{212}Pb peak at 239 keV. This isotope is chosen over ^{208}Tl due to its greater photon emission probability of 43.5%. The same reason dictated the choice of the 911 keV peak of ^{228}Ac, with its photon emission probability of 26.6%, over the 338 keV of ^{228}Ac to calculate the activity of ^{228}Ra (Herranz et al., 2006). Using these 3 peaks, the activities of ^{224}Ra, ^{226}Ra, and ^{228}Ra can be calculated using equation:

$$\left[Ra^{iso}\right] = \frac{\left(\dfrac{peak}{cpm}\right)}{\left(eff \times emm \times mass\right)} \qquad (1)$$

where [Ra^{iso}] refers to the activity of radium isotope being calculated (^{224}Ra, ^{226}Ra, or ^{228}Ra) in dpm/g, peak is the measured peak using the gamma spectrometer (^{212}Pb, ^{214}Pb at 352 keV, or ^{228}Ac at 911 keV), cpm is the counts per minute of the detector, eff is the detector efficiency, and emm is the photon emission probability of the isotope whose peak is being measured. The efficiency or "eff" as it is referred to in Eq. (1) refers to the efficiency of the detector at measuring the peaks present in the sample, which is calculated by running a known standard in the spectrometer and comparing the results to known values (Zielinski and Budahn, 1998).

3.3 X-Ray Fluorescence

X-ray fluorescence (XRF) was used to determine the chemical composition of the studied sediments (Table 1). An XRF spectrometer is an instrument used to perform chemical analyses of rocks, sediments, minerals, and fluids (Potts et al., 2005). Prior to analysis, the sediment is crushed to ~20 μm in size. Sediment samples are then pressed into a 3 cm diameter capsule. In some cases, the quantity of powder is not large enough to fill the entire capsule and therefore another unrelated standard powder is put into the capsule and then covered with the sample. In this case, the sample should homogeneously cover the

exotic powder to ensure the analysis is not contaminated with elements from the other powder. The capsule was then passed through the S-4 XRF Pioneer® spectrometer at the Université de Québec à Montréal for analysis, which determined the average amount of elements in the entire sample ensuring a quantitative chemical analysis of the elements. The uncertainty associated with these results depends in large part on the preparation of the sample. It is estimated that the analytical error can represent up to 90% of the total error.

3.4 X-Ray Diffraction

X-ray diffraction (XRD) analysis is one of the primary techniques used to determine the mineralogical composition of rocks and sediments (Suryanarayana and Norton, 1998). The sediment samples from the core are crushed to about 20 μm in size and several grams are put into the sample holder. If the amount of sample is not sufficient enough to fill the holder, then glue is added prior to the addition of the sample, which is then put into the holder; taking care to ensure that it completely covers the glue. The sample was then put into a Siemens D5000 diffractometer at the Université du Québec à Montréal to determine the mineralogical content of the samples (Table 2). As in the case of X-ray fluorescence, 90% of the analytical error is attributed to the sample preparation technique, while the other 10% is attributed to the orientation of the minerals, which affect the peaks that are recorded.

3.5 Radium Purification and Thermal Ionization Mass Spectroscopy

Water from the wells and hydrothermal springs was collected using a bucket and then left in the bucket for a couple of minutes to cool, as most of the collected waters samples are near boiling point. The water was then poured into a 500 ml container using a funnel. The cap to the container was screwed on and the bottle was labelled with its location's name. The samples were later filtered in the lab with 0.15μm filters to remove particulate. Radium was extracted from the waters according to the procedure outlined by Ghaleb et al. (2004). About 200 ml of the filtered water sample was poured into a 250 ml beaker. An enriched ^{228}Ra spike was added to each weighed water sample. The minimum amount of spike in each sample is ~60 fg. The co-precipitation described by Ghaleb et al. (2004) was performed on these samples. 100 μl of 0.5M $KMnO_4$ was added to the sample. This resulted in the sample turning a purplish colour. The pH of this new purple solution was tested using pH strips and

adjusted to a value of ~8-9 by adding 1M NaOH. 200 µl of 0.5M $MnCl_2 \cdot 4H_2O$ was finally added to start the precipitation MnO_2, which is of a brownish colour. Most of the barium and radium contained in the samples is precipitated with the manganese dioxide, while the remaining liquid contains the calcium and part of the strontium. Ghaleb et al. (2004) explain that it is believed that barium and radium are incorporated onto the manganese dioxide by surface sorption and is pH sensitive. The solution is stirred and left to sit for at least an hour. This allows the precipitate to settle. After sitting, a large part of the liquid is poured out and discarded. The MnO_2 precipitate is recovered by centrifugation. The precipitate is washed with Milli-Q water, centrifuged, dissolved in 5-10 ml of 6M HCl and transferred to a 50 ml Teflon beaker. The solution is heated to 80°C. The reduction of MnO_2 to Mn^{2+} then occurs as evidenced by the gradual disappearance of the brownish colour. When only a slightly brownish colour is left, a few milligrams of a reducing agent (1M absorbic acid) are added to the solution that instantly becomes colourless. The solution is then left to evaporate until it is completely dry. It is then redissolved in 2 ml of 3M HCl. The samples then go through 3 stages of chemical columns: column one gives an eluted fraction of radium and barium, column two gives an eluted fraction of radium and part of the barium, and column three gives simply radium. The final radium fraction is left to dry and then put on a single, zone-refined Re filament with 1 µl of Ta-HF-H_3PO_4. The filament was put into the VG-Sector 54 thermal ionization mass spectrometer at the Université du Québec à Montréal and the radium isotopes and background noise were measured and recorded using a Daly detector in peak jumping mode (Ghaleb et al., 2004).

4. Results

4.1. Chemistry and mineralogy

Major elements analyses carried out by X-ray fluorescence (Table 1) indicated that the deposits are mainly silicic and contain, in decreasing amount, Si (from 11.0 to 25.5 wt%), Al (from 6.5 to 17.7 wt%), S (from 0.1 to 9.6 wt%), and Fe (0.82 to 11.0 wt%). It should be noted that at 39 cm depth in sample 20 there is a calcium peak (8.8 wt%). This is significant as the calcium in the rest of the deposits range from 0.09 to 0.42 wt%. This sample is also of interest as it represents an increase in compositional diversity displaying significant quantities

of Ca (8.8 wt%), K (1.6 wt%), and C (1.2 wt%). There is also a significant decrease in sulfur (0.1 wt%) while the others range from 0.95 wt% to 9.6 wt%. The iron concentration in the core increases with depth from 0.82 wt% at 13 cm up to 11.0 wt% at 43 cm. The iron peaks correspond to the appearance of pyrite in the core: the first peak at 19 cm corresponds to the first appearance of pyrite, while the second peak at 33 cm corresponds to the reappearance of pyrite, which was not present from 19 cm to 33 cm.

From a mineralogical perspective, the core displays several zones of varying mineralogy (Table 2; Fig. 6). The first one is predominantly made-up of the sulfate minerals of the alunite group, which includes alunite ($KAl_3(SO_4)_2(OH)_6$) and natroalunite ($NaAl_3(SO_4)_2(OH)_6$) (occurring when sodium substitutes for potassium in the mineralogical structure of alunite), and extends from the surface to 25 cm depth (sample 13) (Nesse, 2000). Within this zone, there is the first appearance of pyrite and clinoptilolite (($Na,K,Ca)_{2-3}Al_3(Al,Si)_2Si_{13}O_{36} \cdot 12(H_2O)$)) at 19 cm (sample 10). From 27 cm to 29 cm, we find the second zone. This zone is primarily composed of kaolinite ($Al_2Si_2O_5(OH)_4$) and the alunite group minerals. The third zone is found from 31 to 41 cm (samples 16 to 21) and is the most diverse of all zones. This zone contains significant quantities of several minerals, which includes those of the alunite group (from 5.8 to 11.7 wt%), pyrite (from 5.5 to 25.2 wt%), quartz (from 10.4 to 24.9 wt%), clinoptilolite (from 4.3 to 13.4 wt%), kaolinite (from 5.5 to 13.4 wt%), smectite (from 4.0 to 11.7 wt%), cristobalite (from 7.2 to 11.5 wt%), feldspars (from 4.2 to 11.4 wt%), and gypsum ($CaSO_4 \cdot 2H_2O$) (from 2.9 to 8.8 wt%). The final zone starts at 43 cm depth and continues until the end of the core (~50 cm depth). This group is predominately composed of feldspars and pyrite. In this zone, these minerals represent up to 60 wt% of the mineralogy of the sediment.

Several mineralogical trends are observed in the sediments of the core (Fig.6). The concentration of the alunite group minerals decreases with depth. In the first described zone, it represents 80-90 wt% of the sediments of the core. It then decreases to about 35-40 wt% in zone 2. Zone 3 shows a sharp decline in the alunite group minerals, from 50 wt% down to 5 wt%. The final zone, zone 4, contains very little of the alunite group minerals, 2-4 wt%. As previously explained, there is an observed trend between pyrite and the iron concentration

(Fig. 7). Pyrite appears for the first time at a depth of 19 cm and then quickly disappears. At 33 cm, pyrite reappears in the sediments and increases significantly towards the end of the sediment core. It should be noted that the appearance of pyrite coincides with that of clinoptilolite. At 31 cm depth, pyrite also displays an anti-correlation with alunite, which could be accounted for since alunite is a secondary mineral formed with sulfuric acid that itself could be formed during the oxidation of pyrite (Khalaf, 1990). The amount of feldspars increases with depth. They are first found in the sediments in the form of sanidine $((K,Na)(Si,Al)_4O_8)$, a potassium feldspar, at 21 cm (sample 11) and at 29 cm (sample 15). Feldspars are also found in the sample around 37 cm depth and quickly increase in concentration. Towards the end of the sediment core (~50 cm), they represent ~35 wt% of the sediments. The same increase with depth trend is observed with quartz. For the first 29 cm, the quantity of quartz is minimal (0.09 to 6.3 wt%). Afterwards, it increases with depth from 3.86 wt% to a maximum of 24.9 wt%.

Several correlations between chemical elements and minerals present in the core can be made. There is a correlation observed between phosphorus and alunite (Fig.8). Two hypotheses could be made for this correlation: 1) the adsorption of phosphorous by alunite and 2) phosphorus being derived from the aluminium-sulfate-phosphate minerals (Özacar, 2003). Alunite also displays a correlation with strontium (Fig.9). This correlation is thought to be associated to the fact that during the alunitization process, alunite incorporates strontium into its crystalline structure (Stoffregen and Alpers, 1987).

4.2. Radium content

Three radium isotopes (^{224}Ra, ^{226}Ra, ^{228}Ra) were investigated using gamma ray spectrometry (Table 3). When examining ^{224}Ra against depth (Figure 10a), a significant peak is found at 37 cm depth. The isotope displays several trends: a decrease in activity up to 7 cm, an increase from 7 cm to 37 cm, and a decrease from 37 cm until the end of the core. Since ^{228}Ra is part of the same decay chain (^{232}Th) as ^{224}Ra and we expect them to be at secular equilibrium, the same trends should be observed with the ^{228}Ra isotope (Schmidt and Cochran, 2009). To ensure that these isotopes are at secular equilibrium, the ratio of ^{224}Ra/^{228}Ra was plotted against depth (Figure 11). This gave a line close to 1, which

indicated that the system is indeed near secular equilibrium. As expected, the same trends observed with ^{224}Ra are observed with ^{228}Ra (Figure 10b), with the exception that the first zone of decline from the surface continues only to 5 cm depth and this value is very minimal (0.077 dpm/g), which is much smaller than the minimum of ^{224}Ra (0.297 dpm/g). While ^{224}Ra and ^{228}Ra display peaks at 37 cm, ^{226}Ra has a peak at 33 cm. It displays several trends, which differ from those of the radium isotopes of the ^{232}Th decay chain. The ^{226}Ra activity decreases from the surface until 7 cm, it then increases until 17 cm, from there it decreases until 25cm, it then increases to an important maximum at 37 cm, and it then decreases until the end of the core (Figure 10c). When examining the ratio of ^{228}Ra/^{226}Ra (Figure 12), it is difficult to observe a clear trend but three zones were identified: a zone of decrease from the surface to 11 cm, another zone of decreases from 13 to 35 cm, and a final zone of decrease from 37 cm to the end of the core. The ^{210}Pb/^{226}Ra activity ratio was also examined (Figure 13). It was noted that almost all values were below 1 indicating that the age of the system can be calculated using the method developed by Condomines et al. (1999) but it should be noted that in our case, the ratios are not calculated on solely authigenic minerals but rather a mixture of authigenic and inherited material (Gauthier and Condomines, 1999).

Finally, we examined the mineralogy in relation to the results obtained in order to check whether the fluctuations of Ra content with depth could be related to the capacity to be absorbed on certain mineral phases. No such possible link could be inferred. There is no significant variation in the radium isotopes (^{226}Ra and ^{228}Ra). The same holds true for the radium isotopes in comparison to the mineralogy. No mineralogical variation is observed at the two peaks. However, this lack of relation is not surprising as Benes and Srejc (1986) previously noted that the adsorption affinity of the sediments for radium cannot be easily derived from their chemical or mineralogical compositions or other physical properties.

5. Discussion

Condomines et al. (1999) used ^{226}Ra, ^{228}Ra, and their daughter nuclides to estimate the age of several young hydrothermal deposits in the French Massif Central. As discussed earlier, if the hydrothermal deposit is initially devoid of ^{210}Pb, trapped ^{226}Ra should start to

produce ^{210}Pb. Measured $^{210}Pb/^{226}Ra$ should thus increase with time, following the equation (Condomines et al., 1999):

$$\left(^{210}Pb/^{226}Ra\right) = \left(1 - e^{-\lambda_{Pb}t}\right) \qquad (2)$$

Where $\square$ is the decay constant for ^{210}Pb and t is the time. Using these ratios measured in authigenic minerals, the age of the hydrothermal deposit can be estimated (Figure 14). In our case, the ratios were calculated on a mixture of authigenic minerals and one of inherited and altered material, as a result, we can only calculate a maximal age. Using the estimated age of the hydrothermal deposit and the measured $^{210}Pb/^{226}Ra$ ratios, the initial $^{228}Ra/^{226}Ra$ ratio can be calculated. Having calculated these initial $^{228}Ra/^{226}Ra$ ratios, allows us to study the fluctuation of the ratio throughout the deposit (Condomines et al., 1999). This step cannot be accomplished in our case as we do not calculate a real age but only a maximal one.

Using the Condomines et al.'s (1999) method, we attempted to use radium as a geochronometer for the Marítaro hydrothermal springs and to study the fluctuation of the $^{228}Ra/^{226}Ra$ ratio through time. We also attempted to establish a link between the mineralogy, chemical composition, and radium isotopes.

Using equation (2), we were able to calculate maximal ages for the deposits of the hydrothermal springs (Figure 14). By plotting the range of these ages, it can be observed that the majority of the deposits lie within the 20-50 years age bracket (Figure 15). Although these ages are maximum ages, it allows us to conclude that the hydrothermal deposit is very young and was formed throughout the last century.

Condomines et al. (1998) demonstrated that in order to utilize the method, ^{210}Pb should increase with depth as ^{226}Ra decays and produces it. The measured $^{210}Pb/^{226}Ra$ ratios (Figure 13) of the Marítaro hydrothermal springs are all around 0.6 and do not exhibit this trend. Furthermore, the total amount of Ra is extremely low compared those usually measured in hydrothermal deposits (Rhius et al., 1997; Condomines et al., 1998).

The low Ra content could be the result of two possible scenarios:

1- The fluids are depleted in ^{226}Ra;

2 - The ^{226}Ra was not incorporated into the authigenic minerals and remained in the liquid phase and was lost from the system or was incorporated in such a small amount in comparison to the other elements present that it cannot be measured;

The first hypothesis can be immediately discarded. Indeed, as reported in Table 4, we measured radium isotopes in three geothermal wells of the Los Azufres, AZ2, AZ28 (located near Maritaro) and AZ33 and in five hot springs (Bagnes, Chiflador, Currutaco in the south and Araro in the north). Results show that ^{226}Ra activity range from 1902±13 to 16592±307 mBq/l for the springs and from 2810±15 to 51648±358 mBq/l for the geothermal wells. These figures clearly indicated that the fluids are enriched in ^{226}Ra and thus the low radium content in the deposits of Marítaro cannot be due to depletion at the source. Though the amount of radium in the thermal springs and fumaroles is less than in the geothermal brines at depth, it is still present in large amounts, so precipitation of radium at the subsurface, which would leave final fluids depleted in it, can be ruled out.

The ^{226}Ra could not have been retained into mineral phases in the deposits. It should be noted that the studied deposits were silicic at the origin (as indicated by the increased presence of quartz and feldspars at depth), possibly rhyolitic. Occurrence of alunite and kaolinite seems to indicate that rather than deposited from hydrothermal fluids, the studied sediments have been just strongly altered by acidic, sulfur-rich fluids. Yet, sulfates are likely precipitated during the process of alteration and radium shows strong affinities for sulfates (particularly barite). Dickson and Herczeg (1992) measured radionuclides from thermal springs in Australia and clearly showed that alunite-rich bands contained large amounts of Ra thus radium should also have been incorporated in our deposits.

Radium is known to be readily adsorbed onto clays and mineral oxides present in soils, especially near neutral and alkaline pH conditions (Ames et al., 1983; Benes and Strejc, 1986; EPA, 2004). In addition, studies of adsorption and desorption indicate that radium is

essentially completely reversibly adsorbed. Particularly clay minerals and sulfates (barium sulfate) are very good trapping sites of radium in sediments. In addition to the presence of alkaline earth sulfates and metal oxides which influence the sorption of radium, there are a number of other factors that can affect the sorption of materials in general. For example, the affinity of an element for ion exchange relative to other members of its chemical group increases with increasing atomic weight. Therefore, the sorption of radium is the strongest of all the alkaline earth metals. Secondly, given that the number of sites at which ions may be adsorbed are limited, the adsorption of any particular species decreases as the concentration of competing ions increases. In the specific case of radium, its adsorption has been shown to be strongly dependent on ionic strength and concentrations of other competing ions (EPA, 2004). Thirdly, the pH of the system also has a strong effect on the adsorption of cationic species like radium. When an ion is adsorbed onto soil it typically releases a hydrogen ion (H^+). This release is favored under alkaline conditions and inhibited under acidic conditions. Thus, radium will become increasingly mobile in acidic soils and waters. Maritaro effluents are strongly acidic with measured pH of 3.2 (Birkle et al, 2001). Earlier work of Benes and Strejc (1986) showed that for pH lower than 6 the sorption capacity of several minerals drop dramatically to become mostly nil at pH around 3. Thus, the anomalous depletion of radium in our core could be explained by the occurrence of acidic fluids at Maritaro. Though able to create secondary clay minerals and sulfates such as kaolinite and alunite, i.e. good adsorbers, these fluids acidified the system too much hence inhibiting the adsorption of radium.

As previously stated, we were not able to calculate a real date for the springs and therefore could not use Condomines et al.'s (1999) method to determine the initial $^{228}Ra/^{226}Ra$ ratios and therefore study the fluctuations of $^{228}Ra/^{226}Ra$ ratios through time but the fluctuations of the ratio can be examined through depth. The measured $^{228}Ra/^{226}Ra$ ratios range from 0.685 ± 0.091 to 1.513 ± 0.185 with one value at 5 cm depth at 0.122 ± 0.102, which is considered an anomaly being the only point where the $^{224}Ra/^{228}Ra$ ratio departs significantly from unity (Fig. 11). These ratios could indicate how their parents, ^{232}Th and ^{238}U, behave in the hydrothermal springs. There is no clear trend observed and therefore no conclusions can be drawn.

6. Conclusions

The aim of the study was to analyze the ^{226}Ra, ^{228}Ra and ^{210}Pb in order to test whether these isotopes could be used to calculate a chronology of hydrothermal events, following the methodology developed by Condomines et al., (1999). Unfortunately, the very small amount of radium detected and the secular equilibrium attained by the system do not allow us to establish a chronological framework. We are however able to determine a maximum age for the deposits of about 20-50 years. We were also able to clearly show, as demonstrated in previous laboratory experiments (Benes et Streic, 1986), that at very strong acidic conditions (pH<3) the radium adsorption is completely inhibited on clay and sulfate minerals. Thus only on hydrothermal deposits deposited at more neutral or alkaline conditions, such as carbonates of Massif Central (Rihs et al, 1997), the methodology of Condomines can be successfully applied.

7. Acknowledgements

8. References

Adams, J.A. and P.Gasparini. 1970. "Gamma-Ray Spectrometry of Rocks". New York: Elsevier Publishing, p.23-67.

Appleby, P. G., and F. Oldfield. 1978. «The calculation of lead-210 dates assuming a constant rate of supply of unsupported 210Pb to the sediment». CATENA. no 5, p.1-8.

Appleby, P. G., P. J. Nolan, D. W. Gifford, M. J. Godfrey, F. Oldfield, N. J. Anderson and R. W. Battarbee. 1986. «210Pb dating by low background gamma counting, Hydrobiologia». vol 143, no 1, p.21-27.

Arellano, V.M., M.A. Torres and R.M. Barragán. 2005. "Response to Exploitation of the Los Azufres (Mexico) Geothermal Reservoir". Proceedings World Geothermal Congress. Antalya, Turkey, p.1-7.

Benes, P. and P. Strejc. 1986. "Interaction of radium with freshwater sediments and their mineral components". Journal of Radioanalytical and Nuclear Chemistry. vol 99, p.407-422.

Birkle, P., B. Merkel, E. Portugal and I.S. Torres-Alvarado. 2001. "The origin of reservoir fluids in the geothermal field of Los Azufres, Mexico – isotopical and hydrological indications". Applied Geochemistry. vol 16, p.1595-1610.

Condomines M., C. Brouzes and S. Rhis. 1999. «Radium and its daughters in hydrothermal carbonates from Auvergne (French Massif Central): origin and dating applications». Comptes Rendus de l'Academie des Sciences Series IIA Earth and Planetary Science. vol 328, p.23-28.

Condomines M., S. Rihs, E. Lloret and J.L. Seidel. 2010. «Determination of the four natural Ra isotopes in thermal waters by gamma-ray spectrometry». Applied Radiation and Isotopes. vol 68, p.384–391.

Dickson, B. L. and A.L. Herczeg. 1992. "Deposition of trace elements and radionuclides in the spring zone, Lake Tyrrell, Victoria, Australia". Chemical Geology. vol 96, p.151-166.

Ferrari, L., V.H. Garduño, G. Pasquarè and A. Tibaldi. 1991. «Geology of Los Azufres Caldera, Mexico, and its relationships with regional tectonics». Journal of Volcanology and Geothermal Research. vol 47, no 1-2, p. 129-148.

Gauthier, P.G. and M. Condomines. 1999. "210Pb-226Ra radioactive disequilibria in recent lavas and radon degassing: interferences on the magma chamber dynamics at Stromboli and Merapi volcanoes". Earth and Planetary Science Letters. vol 172, p.111-126.

Ghaleb, B., E. Pons-Branchu and P. Deschamps. 2004. «Improved method for radium extraction from environmental samples and its analysis by thermal ionization mass spectrometry». Journal of Analytical Atomic Spectrometry. vol 19, p.906-910.

González-Partida, E., P. Birkle and I.S. Torres-Alvarado. 2000. "Evolution of the hydrothermal system at Los Azufres, Mexico, based on petrologic, fluid inclusion and isotopic data". Journal of Volcanology and Geothermal Research. vol 104, p.277-296.

González-Partida, E., A. Carrillo-Chávez, G. Levresse, E. Tello-Hinojosa, S. Venegas-Salgado, G. Ramirez-Silva, M. Pal-Verma, J. Tritlla, and A. Camprubi. 2005. «Hydro-geochemical and isotopic fluid evolution of the Los Azufres geothermal field, Central Mexico». Applied Geochemistry. vol 20, p.23-39.

Herranz, M., R. Idoeta, A. Abelairas, and F. Legarda. 2006. "Radon fixation for determination of 224Ra, 226Ra and 228Ra via gamma-ray spectrometry". Radiation Measurements. vol 41. p.486-491.

Khalaf, F., 1990. "Diagenetic alunite in clastic sequences, Kuwait, Arabian Gulf". Sedimentology. vol 37, p.155-164.

Nesse, W. D. 2000. *Introduction to Mineralogy*. New York: Oxford University Press, p.342.

Pandarinath, K., P. Dulski, I.S. Torres-Alvarado and S.P. Verma. 2008. "Element mobility during the hydrothermal alteration of rhyolitic rocks of the Los Azufres geothermal field, Mexico". Geothermics. vol 37, p.53-72.

Potts, P.J., A.T. Ellis, P. Kregsamer, C. Streli, C. Vanhoof, M. West, and P. Wobrauschek. 2005. "Atomic spectrometry update. X-Ray fluorescence spectrometry". Journal of Analytical Atomic Spectrometry. vol 20, p.1124-1154.

Özacar, M. 2003. "Adsorption of phosphate from aqueous solution onto alunite". Chemosphere. vol 51, no 4, p.321-327.

Rihs, S., M. Condomines and Ch. Fouillac. 1997. «U- and Th-series radionuclides in CO2-rich geothermal systems in the French Massif Central». Journal of Radioanalytical and Nuclear Chemistry. vol 226, p.149-157.

Rihs, S. and M. Condomines. 2002. «An improved method for Ra isotope (226Ra, 228Ra, 224Ra) measurements by gamma spectrometry in natural waters: application to CO2-rich thermal waters from the French Massif Central». Chemical Geology. vol 182, p.409-421.

Schmidt, S. and J.K. Cochran 2009. "Radium and radium-daughter nuclides in carbonates: a brief overview of strategies for determining chronologies". Journal of Environmental Radioactivity. vol 101, no 7, p.530-537.

Stoffregen, R.E. and C.N. Alpers. 1987. "Woodhouseite and svanbergite in hydrothermal ore deposits: products of apatite destruction during advanced argillic alteration". Canadian Mineralogist. vol 25, p.201-211.

Suryanarayana, C. and M.G. Norton. 1998. *X-Ray Diffraction: A Practical Approach*. New York: Plenum Press, p.80-84.

Verma, S.P., I.S. Torres-Alvarado, M. Satir, and P.F. Dobson. 2005. "Hydrothermal alteration effects in geochemistry and Sr, Nd, Pb and O isotopes of magmas from the Los Azufres geothermal field (Mexico): A statistical approach". Geochemical Journal. vol 39. p.141-163.

Zielinski, R.A. and J.R. Budahn. 1998. "Radionuclides in fly ash and bottom ash: improved characterization based on radiography and low energy gay-ray spectrometry". Fuel. vol 77, no 4, p. 259-267.
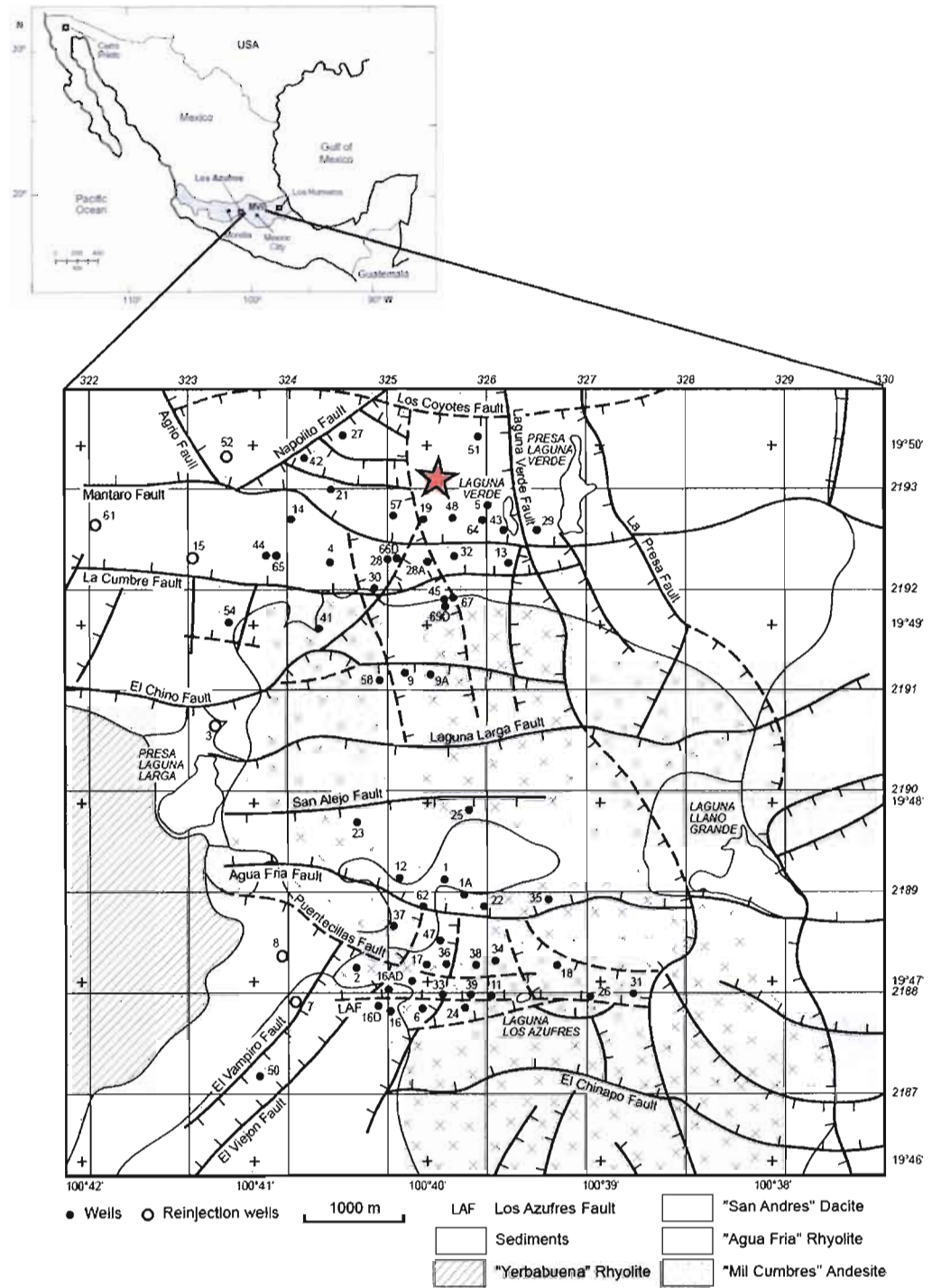
Figure 1. Location of the Maritaro hydrothermal springs within the Los Azufres Geothermal Field and Mexico
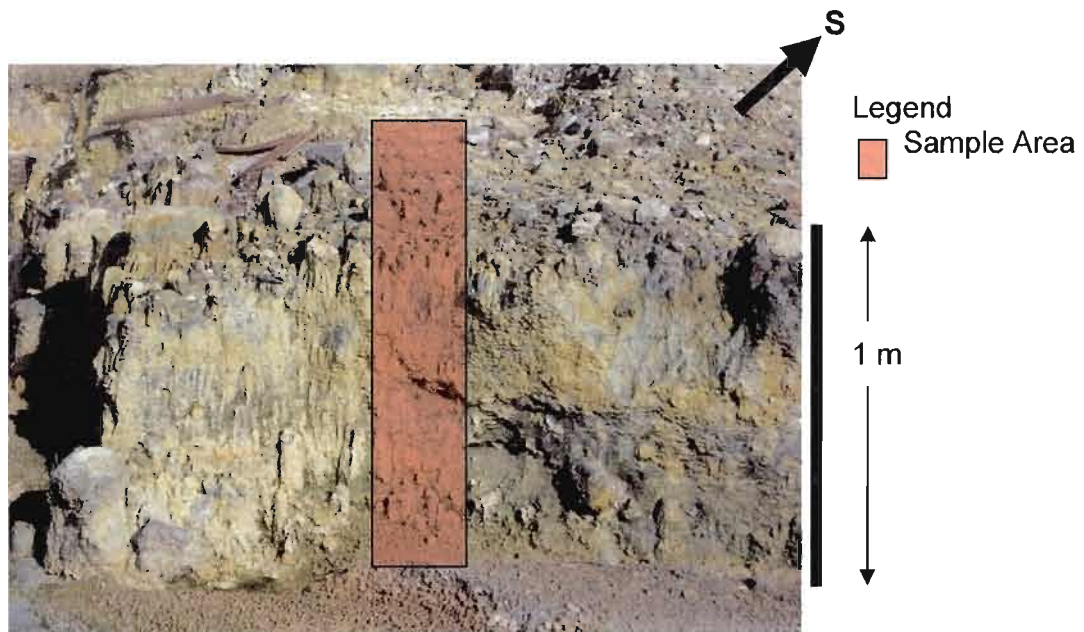
Figure 2. Picture of hydrothermal deposit in the Maritaro hydrothermal springs where the core was extracted
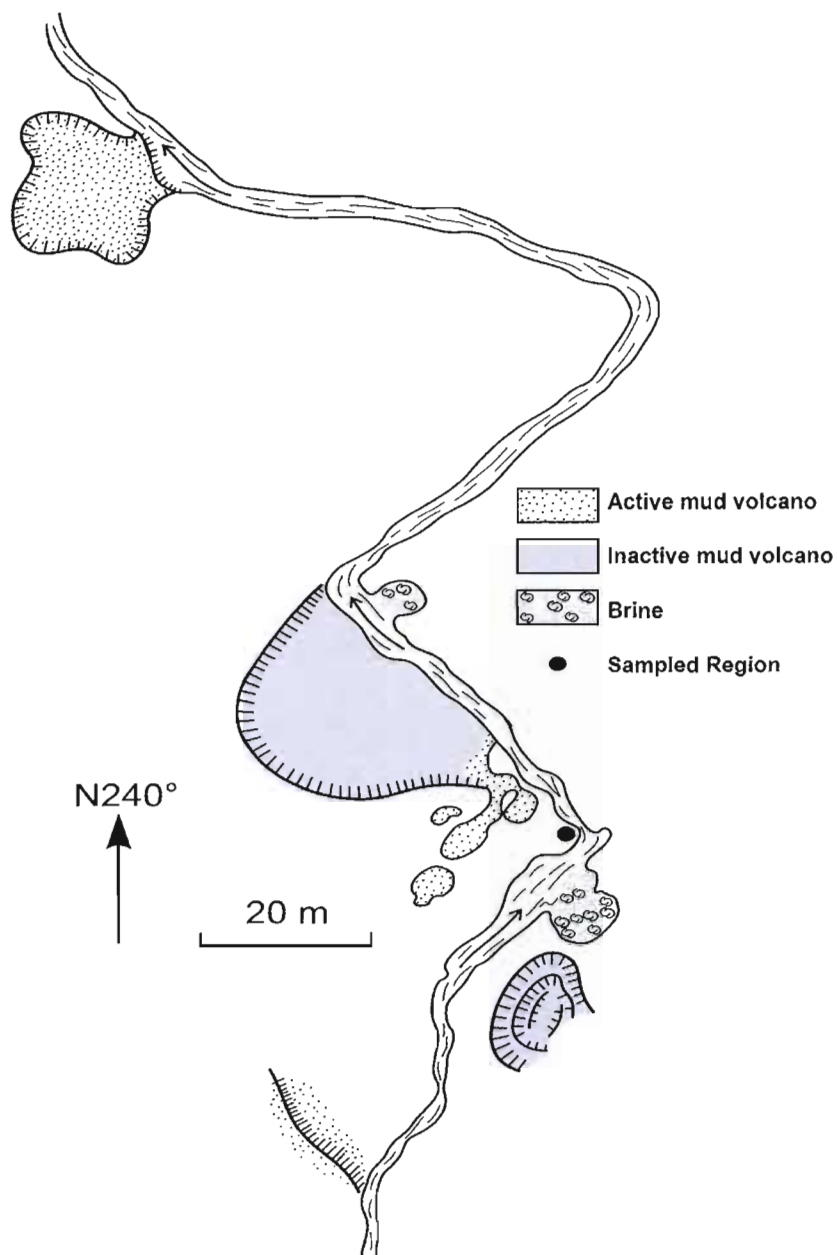
Figure 3. Location within the Maritaro hydrothermal springs where the core was extracted

Figure 4. Picture of the core extracted from the Maritaro hydrothermal springs

U 92	^{238}U 4.47·10^9 yr		^{234}U 2.45·10^5 yr				
Pa 91		^{234}Pa 1.17min					
Th 90	^{234}Th 24.1 d		^{230}Th 7.54·10^4 yr				
Ac 89							
Ra 88			^{226}Ra 1600 yr				
Fr 87							
Rn 86			^{222}Rn 3.82 d				
At 85							
Po 84			^{218}Po 3.04 min		^{214}Po 1.64·10^{-4}s		^{210}Po 138.4d
Bi 83				^{214}Bi 19.7min		^{210}Bi 5.01d	
Pb 82			^{214}Pb 26.9 min		^{210}Pb 22.6 yr		^{206}Pb
Tl 81				^{210}Tl 1.3 min		^{206}Tl 4.20min	

Figure 5a. Decay chain of ^{238}U, where vertical arrows represent α decay and diagonal ones represent β^- decay. Half-lives are indicated under each isotope.

U 92					
Pa 91					
Th 90	^{232}Th $1.40 \cdot 10^{10}$ yr		^{228}Th 1.91 yr		
Ac 89		^{228}Ac 6.15 hr			
Ra 88	^{228}Ra 5.76 yr		^{224}Ra 3.66 d		
Fr 87					
Rn 86			^{220}Rn 55.6 s		
At 85					
Po 84			^{216}Po 0.15 s		^{212}Po $3 \cdot 10^{-7}$ s
Bi 83				^{212}Bi 60.5 min	
Pb 82			^{212}Pb 10.6 hr		^{208}Pb
Tl 81				^{208}Tl 3.1 min	

Figure 5b. Decay chain of ^{232}Th, where vertical arrows represent α decay and diagonal ones represent β^- decay. Half-lives are indicated under each isotope.
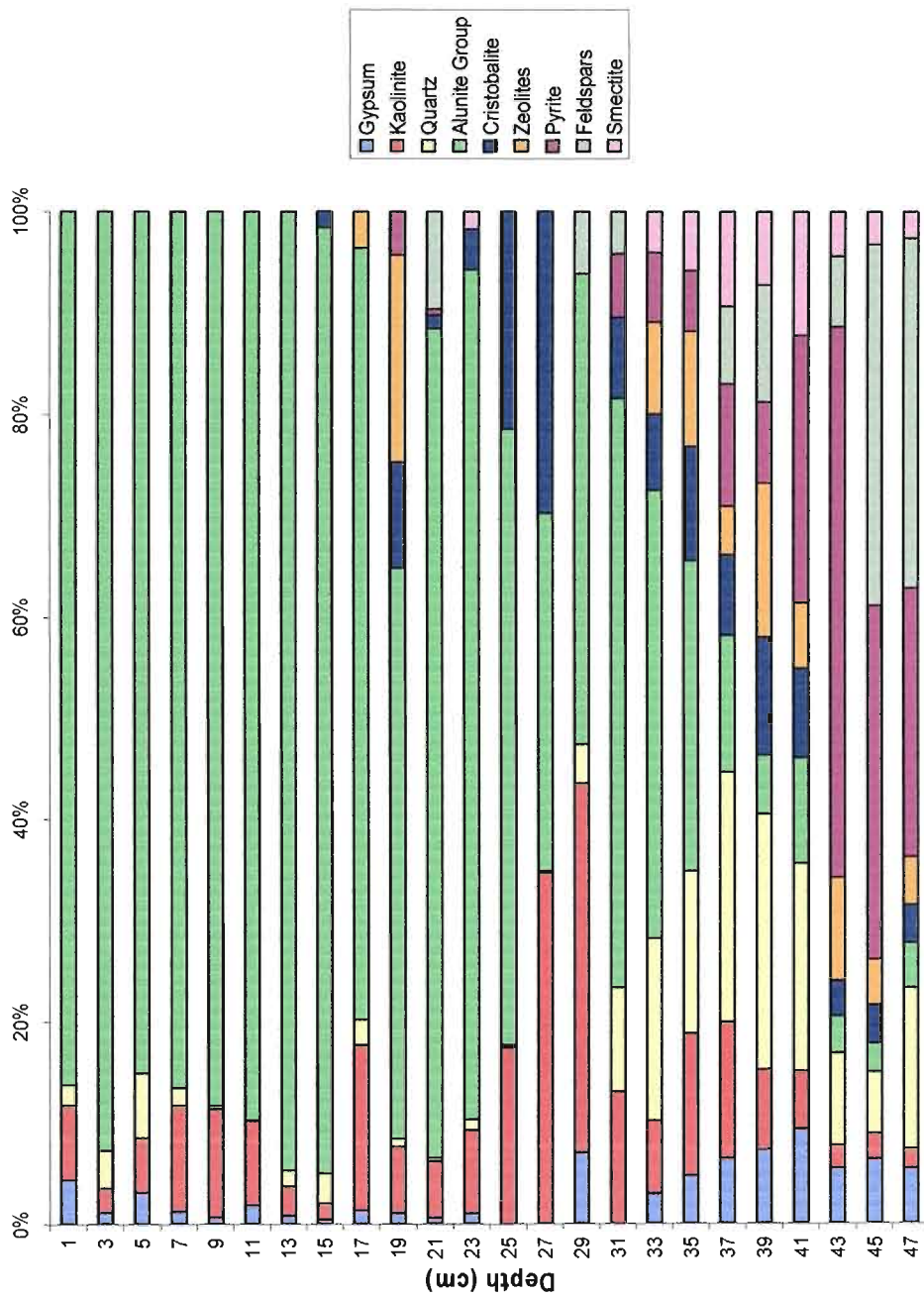
Figure 6. Mineralogy of the core
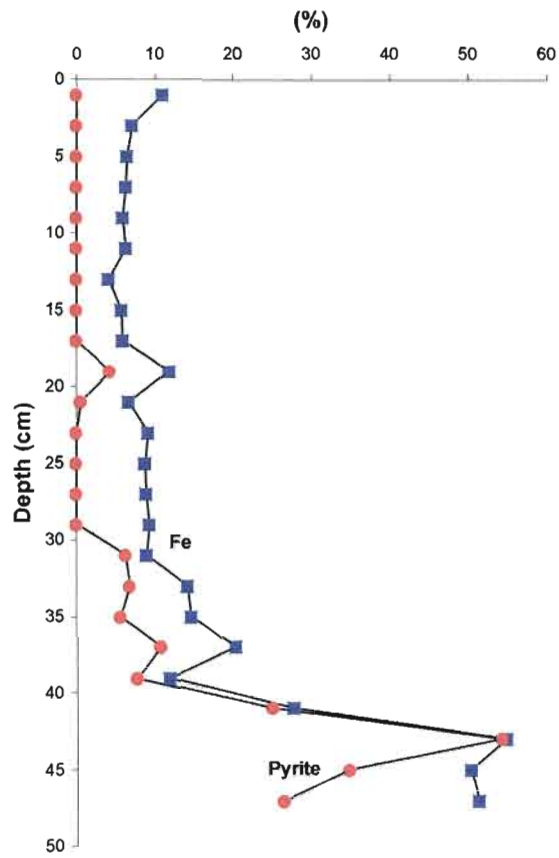
Figure 7. Correlation between pyrite and iron within the core
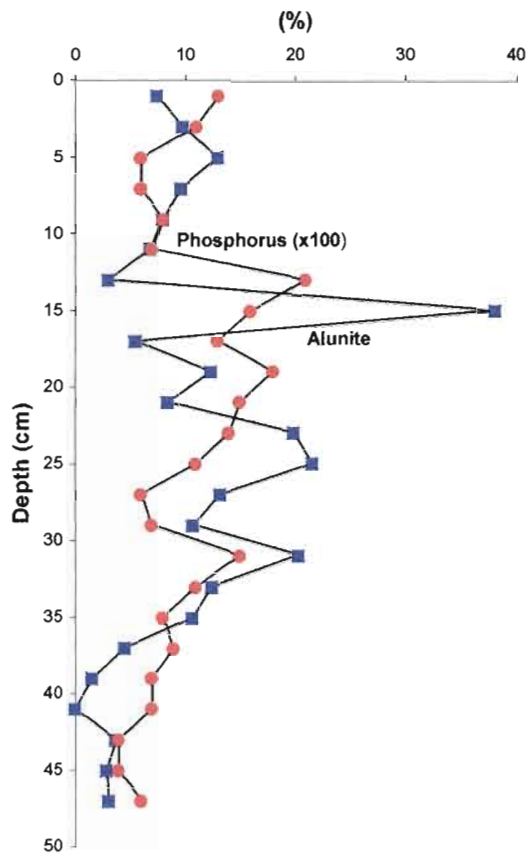
Figure 8. Correlation between phosphorus and alunite within the core
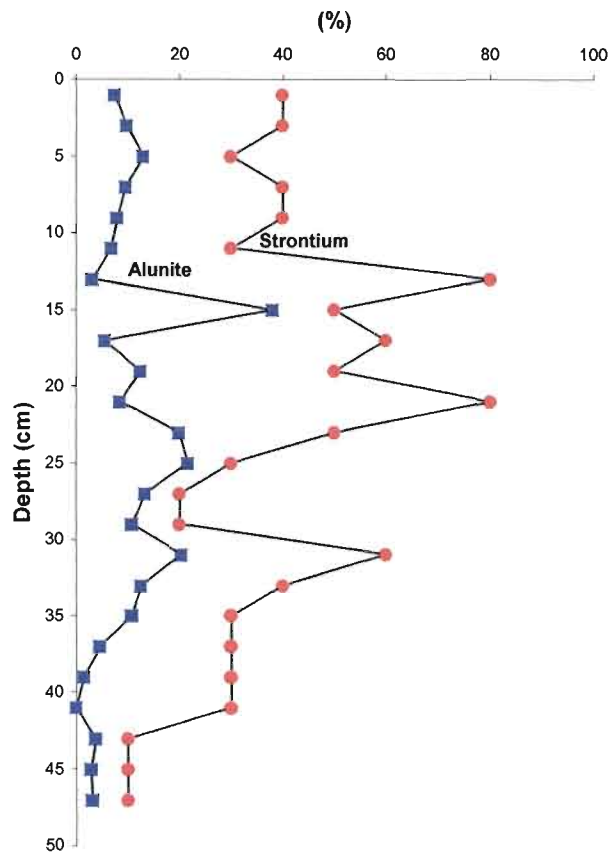
Figure 9. Correlation between strontium and alunite within the core
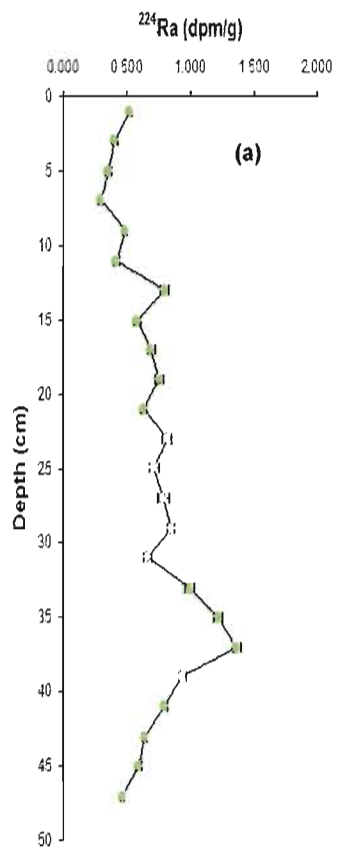
Figure 10a. ^{224}Ra vs. depth
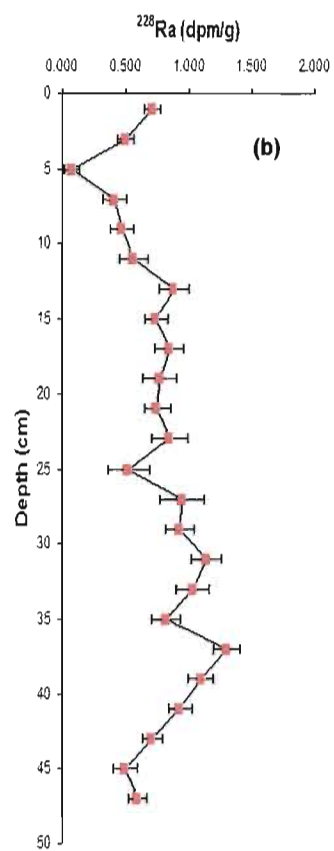
Figure 10b. ^{228}Ra vs. depth
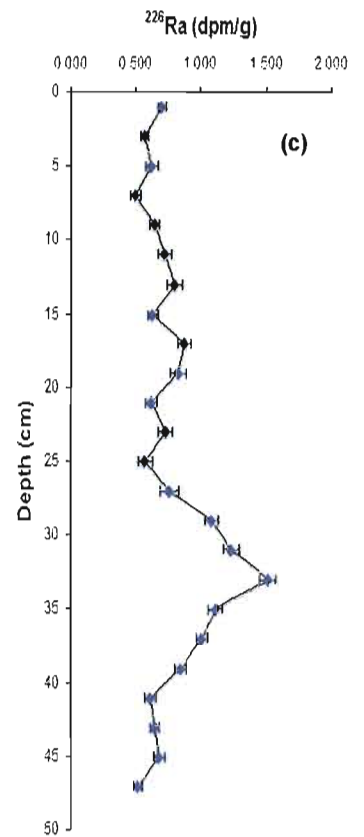
Figure 10c. ^{226}Ra vs. depth
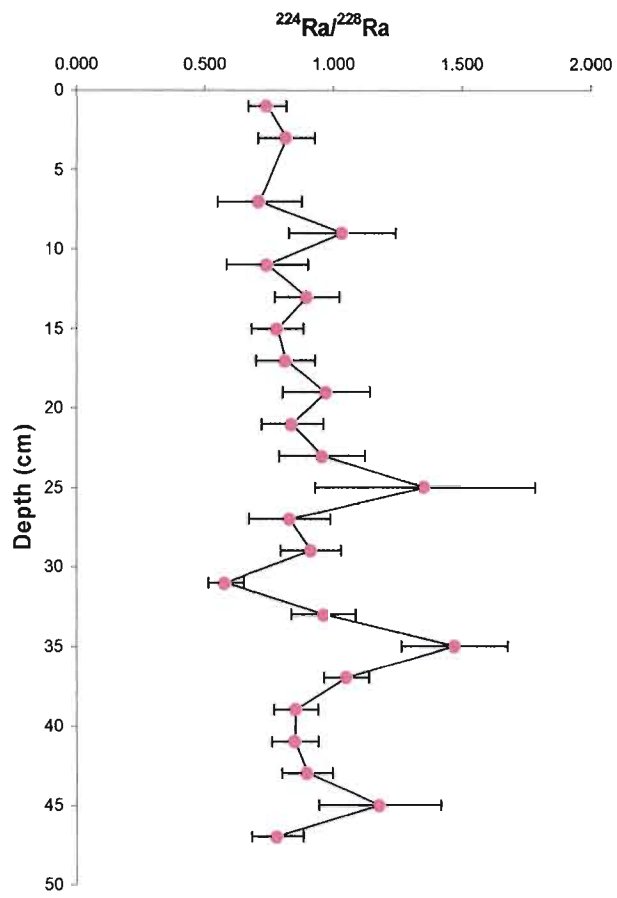
Figure 11. ^{224}Ra/^{228}Ra vs. depth
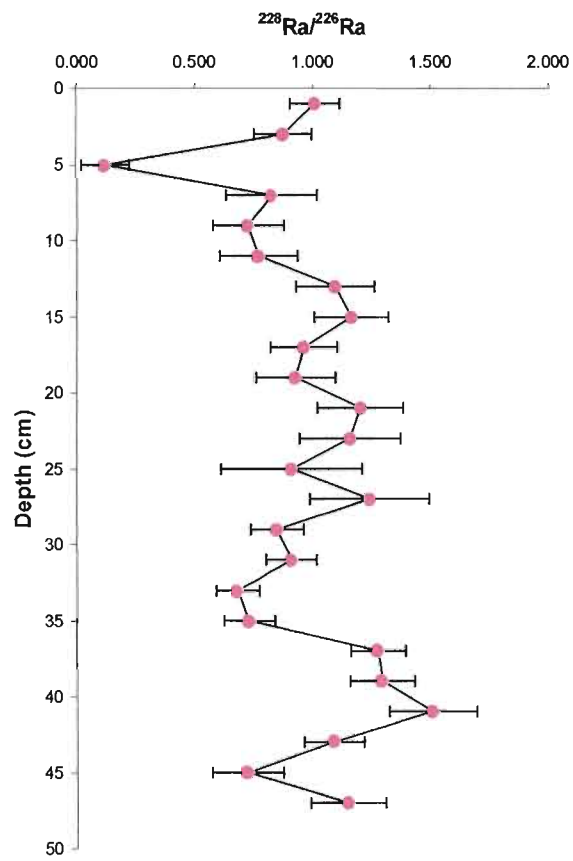
Figure 12. ^{228}Ra/^{226}Ra vs. depth
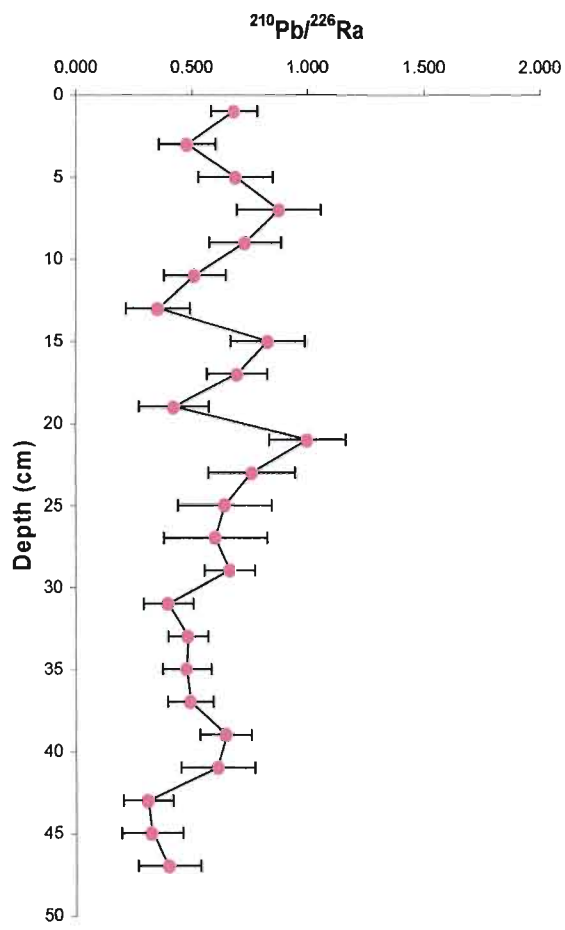
Figure 13. ^{210}Pb/^{226}Ra vs. depth
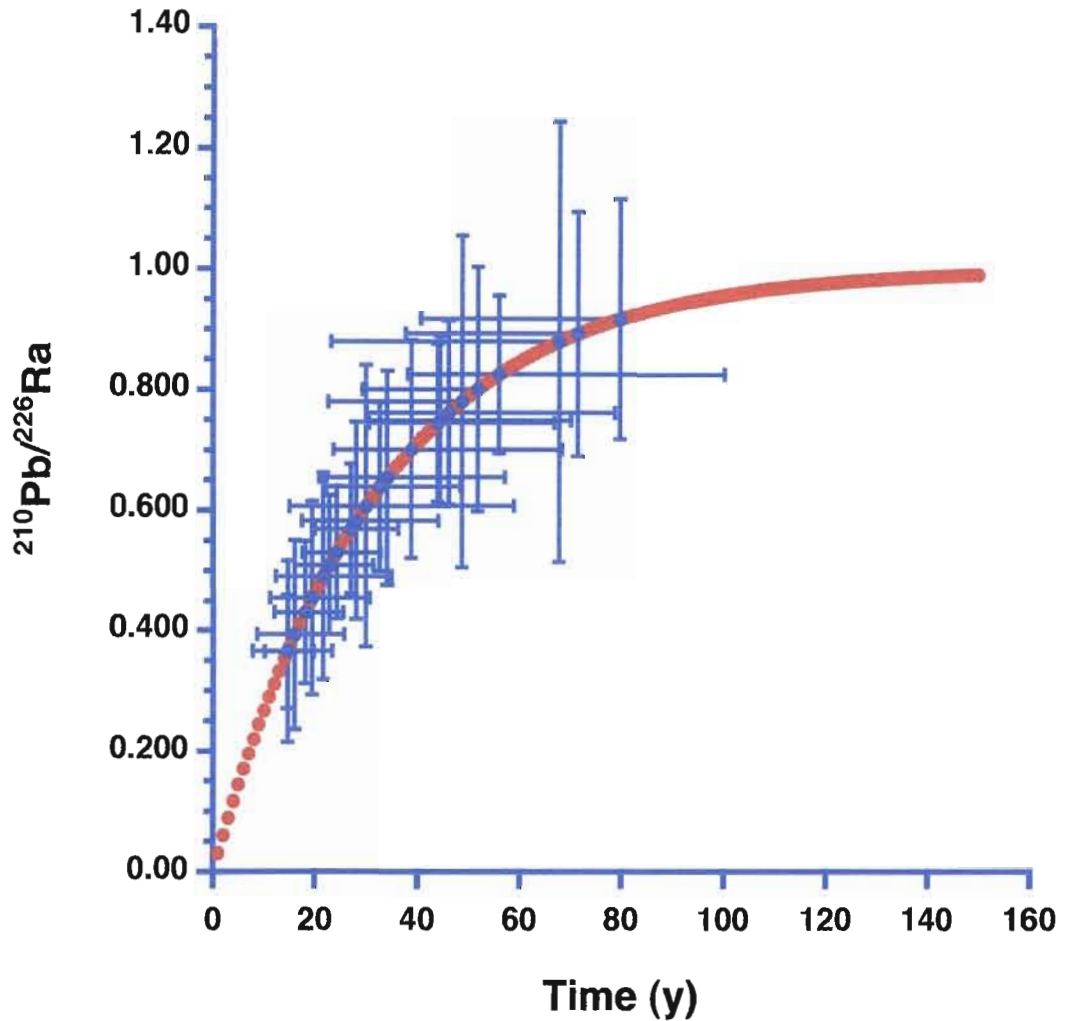
Figure 14. Calculated dates of the sediments from the core of the Maritaro hydrothermal springs calculated using the method of Condomines et al. (1999) represented by the blue points and the ^{210}Pb vs. depth curve as calculated by Condomines et al. (1999) represented by the red line
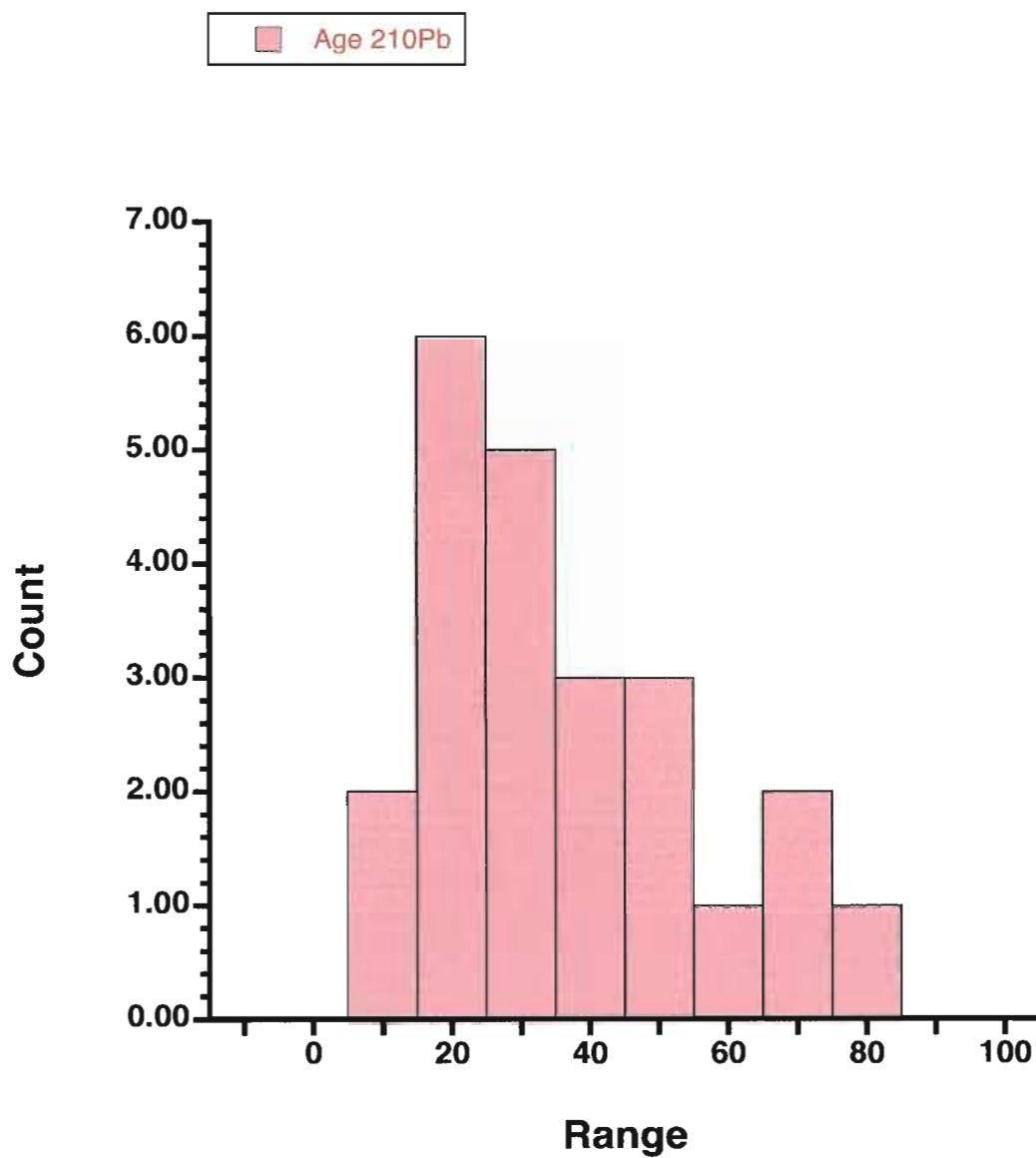
Figure 15. Range of calculated ages present in the sediments of the core obtained from the Maritaro hydrothermal springs

Table 1. Chemical elements present in the core

| Sample	Depth (cm)	O (%)	Si (%)	Al (%)	S (%)	Fe (%)	K (%)	Ti (%)	Na (%)	Mg (%)	Ca (%)	Sr (%)	Ba (%)	P (%)
1	1	55.90	15.50	15.90	6.62	2.19	1.06	0.77	1.24	0.20	0.23	0.04	0.04	0.13
2	3	55.30	22.20	14.10	3.86	1.42	0.79	1.00	0.72	0.17	0.13	0.04	0.06	0.11
3	5	55.50	25.40	13.50	2.03	1.29	0.41	1.00	0.34	0.21	0.11	0.03	0.06	0.06
4	7	55.80	22.80	13.40	2.49	1.26	0.54	0.73	0.40	0.25	0.09	0.04	0.06	0.06
5	9	55.70	22.10	15.00	3.29	1.18	0.67	0.72	0.62	0.25	0.13	0.04	0.09	0.08
6	11	55.80	21.90	15.80	2.83	1.26	0.65	0.65	0.51	0.27	0.11	0.03	0.11	0.07
7	13	55.60	11.00	17.70	9.60	0.82	1.42	0.44	2.62	0.09	0.21	0.08	0.05	0.21
8	15	55.10	18.00	15.80	6.00	1.15	1.00	0.79	1.55	0.12	0.19	0.05	0.05	0.16
9	17	55.30	21.70	14.80	3.83	1.18	0.93	0.84	0.78	0.12	0.16	0.06	0.06	0.13
10	19	54.80	20.90	16.00	3.24	2.36	0.85	0.71	0.34	0.31	0.14	0.05	0.09	0.18
11	21	55.40	16.60	16.30	6.35	1.34	1.44	0.65	1.30	0.10	0.18	0.08	0.07	0.15
12	23	55.60	20.20	15.20	3.96	1.83	0.92	0.79	0.77	0.17	0.17	0.05	0.05	0.14
13	25	55.40	24.90	13.50	1.97	1.75	0.69	0.91	0.16	0.29	0.11	0.03	0.04	0.11
14	27	55.30	25.50	14.60	0.95	1.78	0.38	0.86	0.21	0.15	0.09	0.02	0.02	0.06
15	29	55.40	24.40	15.00	1.34	1.86	0.44	0.82	0.21	0.21	0.09	0.02	0.03	0.07
16	31	55.40	21.60	15.60	2.99	1.79	0.84	0.75	0.22	0.34	0.13	0.06	0.07	0.15
17	33	54.70	23.40	14.00	2.56	2.82	0.60	0.78	0.18	0.37	0.17	0.04	0.10	0.11
18	35	54.50	24.30	13.90	2.07	2.92	0.45	0.89	0.11	0.39	0.15	0.03	0.08	0.08
19	37	54.20	22.90	14.20	2.22	4.07	0.33	0.98	0.08	0.50	0.20	0.03	0.07	0.09
20	39	52.80	23.90	6.53	0.10	2.40	1.60	0.42	1.04	0.98	8.81	0.03	0.03	0.07
21	41	53.10	22.90	12.00	3.53	5.57	0.59	0.85	0.21	0.69	0.33	0.03	0.04	0.07
22	43	48.40	19.60	9.42	9.13	11.00	0.51	0.57	0.29	0.60	0.41	0.01	0.03	0.04
23	45	49.10	21.50	8.29	8.41	10.10	0.53	0.64	0.33	0.56	0.40	0.01	0.03	0.04
24	47	50.20	20.30	7.74	8.76	10.30	0.58	0.57	0.40	0.56	0.40	0.01	0.03	0.06

Table 2. Mineralogy of the core

Sample	Depth (cm)	Gypsum (%)	Kaolinite (%)	Quartz (%)	Alunite (%)	Natroalunite (%)	Cristobalite (%)	Natrolite (%)	Clinoptilolite (%)	Pyrite (%)	Sanidine (%)	Smectite (%)	Feldspars (%)
1	1	4.37	7.34	2.02	7.42	78.83	-	-	-	-	-	-	-
2	3	1.15	2.41	3.72	9.75	82.97	-	-	-	-	-	-	-
3	5	3.13	5.39	6.35	12.94	72.20	-	-	-	-	-	-	-
4	7	1.27	10.42	1.70	9.60	77.00	-	-	-	-	-	-	-
5	9	0.70	10.64	0.33	7.96	80.36	-	-	-	-	-	-	-
6	11	1.89	8.25	0.09	6.83	82.95	-	-	-	-	-	-	-
7	13	0.82	2.88	1.56	3.07	91.67	-	-	-	-	-	-	-
8	15	0.43	1.62	2.93	38.04	55.41	1.57	-	-	-	-	-	-
9	17	1.35	16.28	2.54	5.53	70.74	-	3.57	-	-	-	-	-
10	19	1.07	6.54	0.77	12.39	44.06	10.46	-	20.43	4.28	-	-	-
11	21	0.60	5.55	0.34	8.48	73.50	1.33	-	-	0.59	9.63	-	-
12	23	1.00	8.21	1.02	19.86	64.18	3.96	-	-	-	-	1.76	-
13	25	-	17.41	0.25	21.57	39.31	21.46	-	-	-	-	-	-
14	27	-	34.73	0.18	13.23	22.18	29.86	-	-	-	-	-	-
15	29	6.95	36.55	3.86	10.74	35.80	-	-	-	-	6.10	-	-
16	31	-	12.93	10.36	20.30	37.96	7.96	-	-	6.30	-	-	4.17
17	33	2.89	7.13	17.90	12.48	31.51	7.45	1.09	7.94	6.83	-	4.00	-
18	35	4.49	13.40	15.35	10.70	18.64	10.77	-	10.90	5.68	-	5.56	-
19	37	5.78	12.10	22.37	4.56	7.59	7.20	-	4.34	10.86	-	8.42	6.96
20	39	7.18	7.80	24.85	1.55	4.24	11.46	1.63	13.42	7.88	-	7.10	11.43
21	41	8.83	5.46	19.60	-	9.95	8.37	-	6.23	25.17	-	11.65	-
22	43	5.43	2.25	9.06	3.73	-	3.49	5.62	4.64	54.40	-	4.41	6.97
23	45	6.29	2.52	6.08	2.87	-	3.80	2.31	2.19	35.00	-	3.20	35.74
24	47	5.38	1.91	15.95	3.06	1.38	3.76	2.71	2.05	26.59	-	2.61	34.61

Table 3. ^{224}Ra ^{226}Ra ^{228}Ra and ^{210}Pb in the core

Sample	Depth (cm)	^{228}Ra/^{226}Ra	±	^{210}Pb/^{226}Ra	±	^{224}Ra/^{228}Ra	±
1	1	1.010	0.106	0.684	0.099	0.743	0.074
2	3	0.876	0.121	0.481	0.124	0.819	0.109
3	5	0.122	0.102	0.690	0.161	4.620	3.835
4	7	0.828	0.193	0.878	0.182	0.714	0.164
5	9	0.730	0.150	0.731	0.154	1.036	0.209
6	11	0.774	0.165	0.513	0.135	0.744	0.158
7	13	1.099	0.166	0.355	0.139	0.898	0.125
8	15	1.167	0.158	0.830	0.162	0.784	0.100
9	17	0.966	0.141	0.696	0.130	0.816	0.115
10	19	0.931	0.169	0.423	0.152	0.973	0.169
11	21	1.206	0.182	1.000	0.165	0.840	0.119
12	23	1.161	0.214	0.760	0.187	0.958	0.166
13	25	0.914	0.298	0.643	0.203	1.357	0.427
14	27	1.244	0.253	0.603	0.224	0.831	0.158
15	29	0.853	0.113	0.665	0.109	0.913	0.117
16	31	0.913	0.108	0.399	0.107	0.583	0.069
17	33	0.685	0.091	0.485	0.087	0.962	0.125
18	35	0.736	0.107	0.479	0.105	1.472	0.207
19	37	1.281	0.116	0.495	0.099	1.051	0.088
20	39	1.298	0.138	0.647	0.111	0.855	0.085
21	41	1.513	0.185	0.614	0.159	0.852	0.090
22	43	1.093	0.128	0.312	0.106	0.898	0.099
23	45	0.728	0.150	0.327	0.132	1.181	0.237
24	47	1.154	0.160	0.403	0.136	0.782	0.100

Table 4. ^{226}Ra values in the waters of the Los Azufres geothermal wells

Locality	Type	^{226}Ra (mBq/l)	±
AZ28	Well	2810	15
Araro North	Spring	1981	21
AZ33	Well	51648	358
AZ2	Well	16592	307
Bagnes 2	Spring	6703	82
Currutaco	Spring	16592	307
Chiflador	Spring	1902	13
Bagnes 2	Spring	7967	2437

CONCLUSION GÉNÉRALE

Le but de cette étude était de mesurer les isotopes de ^{226}Ra, ^{228}Ra, et ^{210}Pb afin de déterminer s'ils pouvaient être utilisés pour déterminer la chronologie des événements hydrothermaux des dépôts de Maritaro dans le champ géothermique de Los Azufres par la méthode de Condomines et al. (1999). Cette méthode utilise le rapport de ^{210}Pb/^{226}Ra pour établir une chronologie des dépôts hydrothermaux. La faible quantité mesurée de radium, le fait que les dépôts soient composés d'un mélange de minéraux authigènes, matières altérées et matières héritées et que l'équilibre séculaire ait été atteint, ne permettent pas de déterminer une chronologie exacte, mais nous permet d'estimer un âge maximum pour les dépôts de 20 à 50 ans. Cette étude nous a aussi permis de confirmer les études de Benes et Streic (1998) montrant que dans des conditions très acide (pH<3), le radium ne peut pas être complètement absorbé sur des minéraux de sulfates et d'argiles. On peut donc conclure qu'on peut utiliser la méthodologie de Condomines et al. (1999) seulement sur des dépôts hydrothermaux ayant été formés sous des conditions de pH neutre ou alcalin. Finalement, nous n'avons trouvé aucun lien entre la composition minéralogique et chimique des sédiments analysés et les isotopes du radium, indiquant une absence de contrôle minéralogique dans la distribution de ces radionucléides dans les sols.

ANNEXE A

DONNÉES STRONTIUM

En janvier 2009, nous avons échantillonné les eaux de 6 puits du champ
géothermique Los Azufres (AZ1, AZ9, AZ22, AZ28, AZ51, et AZ62) et 2 sources
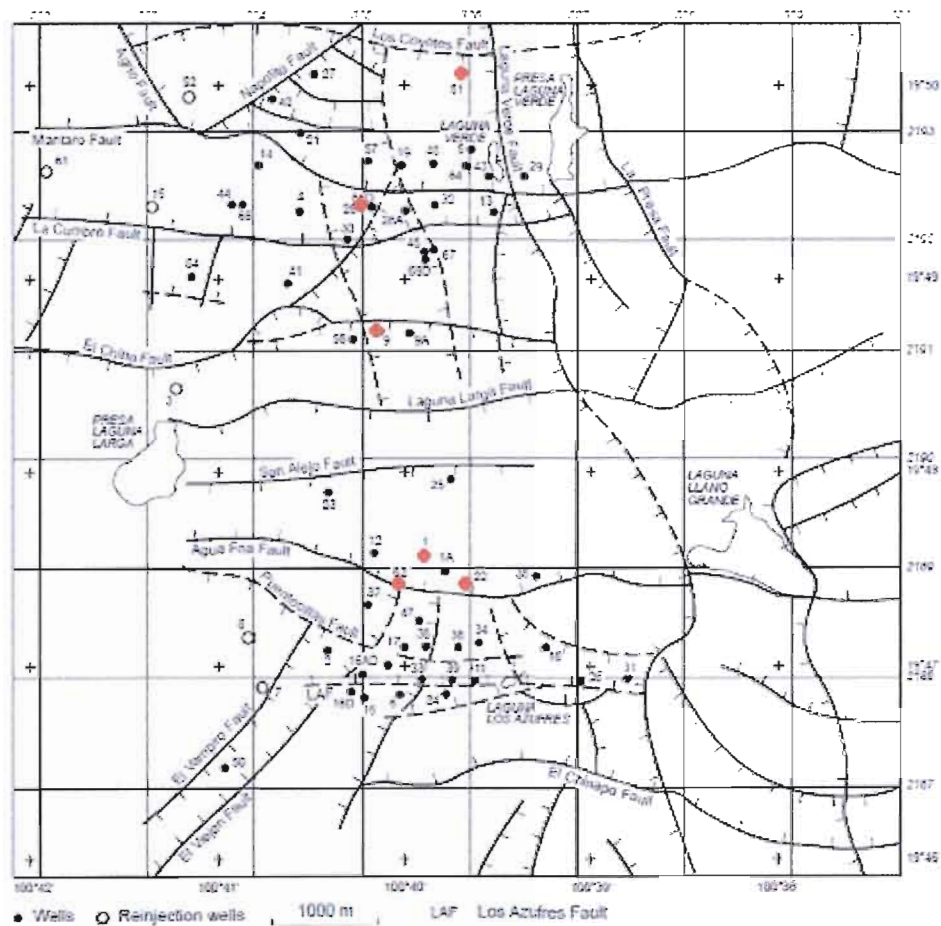hydrothermales (Araro Nord et Maritaro) (Fig.A.1).

Figure A.1. Carte du champ géothermique Los Azufres avec la position de tous les puits

La source hydrothermale de Araro est situé ~ 30 km au nord-ouest du champ géothermique Los Azufres à l'extérieur de la caldera (Segovia et al, 2005). Le but était d'étudier les isotopes du strontium parmi les autres isotopes dans ces eaux pour déterminer leurs sources potentielles et vérifier si ces eaux sont connectées hydrauliquement au réservoir principal de Los Azufres. Les isotopes du strontium peuvent être utilisés dans des milieux hydrothermaux car ils dépendent des interactions entre l'eau, les réservoirs rocheux et le mélange de fluides de différentes compositions isotopiques (Anschutz et al., 1995).

Pour échantillonner ces eaux, on a utilisé un sceau métallique. Plusieurs minutes ont été attendues pour que l'eau se refroidisse. Utilisant un entonnoir, on a versé l'eau dans un conteneur de 500 ml. Après le retour à Montréal, les échantillons ont été envoyés à l'Université de Waterloo où les isotopes de strontium ($^{87}Sr/^{86}Sr$) ont été déterminés. Les résultats se trouvent dans le tableau A.1.

Puits/Sources hydrothermales	$^{87}Sr/^{86}Sr$	±
AZ1	0.70565	0.00005
AZ9	0.70458	0.00005
AZ22	0.70424	0.00006
A28	0.70475	0.00004
AZ51	0.70411	0.00004
AZ62	0.70440	0.00004
Araro Nord	0.70402	0.00004
Maritaro	0.70486	0.00004

Tableau A.1. Résultats de $^{87}Sr/^{86}Sr$ pour les puits et sources hydrothermales mesurés par TIMS

Nos résultats de $^{87}Sr/^{86}Sr$ pour les puits sont de 0.70411±0.00004 à 0.70565±0.00005 et ceux des sources hydrothermales sont de 0.70402±0.00004 à 0.70486±0.00004. En comparant nos résultats à ceux d'autres sources (Tab.A.2), on aperçoit qu'un enrichissement en strontium radiogénique, par rapport à un source magmatique de type MORB (0.70265-0.70308) est à envisager.

Source	$^{87}Sr/^{86}Sr$
MORB	0.70265-0.70308*
Eau de mer récente	0.70916**
Radiogénique	0.72955***
Volcans jeunes	~0.703****

Tableau A.2. Résultats de $^{87}Sr/^{86}Sr$ pour d'autres sources (* - Johnson et Arculus, 1978; ** - DePaolo et Ingram, 1985; ***- Barrat et al., 2000; ****- Åberg, 1994)

Verma et al. (2007) ont mesuré des valeurs de 0.7050 dans les rhyolites et dacites qui constituent le dernière épisode volcanique de la région, daté entre 1 et 0.15 Ma. Donc les eaux échantillonnées dans cette étude pourraient avoir lessivé ces roches en acquérant une signature de strontium plus radiogénique (augmentant le ^{87}Sr). On voit aussi que le ratio $^{87}Sr/^{86}Sr$ de la source hydrothermale d'Araro (0.70402±0.00004) est cohérent avec les rapports des autres puits de la région de champ géothermale Los Azufres. Avec ces résultats, on peut déterminer que nous ne pouvons pas exclure l'hypothèse qu'Araro provient de la même source que les puits et sources de la région du champ géothermal Los Azufres. Néanmoins, ces résultats ne sont pas discutés dans l'article ci-joint mais sont cependant très intéressants pour mieux comprendre les interactions entre les fluides géothermaux et la roche encaissante.

ANNEXE B

DONNÉES RADIUM

En 2008, les eaux de 3 puits (AZ2, AZ8, et AZ33) et 4 sources hydrothermales (Araro Nord, Bagnes, Chiflador et Currutaco) ont été échantillonnées (Fig.A.1). Tous ces puits et sources, sauf Araro, font partie du système de Los Azufres. Araro est situé environ 30 km nord-ouest du champ géothermal Los Azufres (Segovia et al., 2005). Ces eaux ont été analysées pour déterminer leur teneur en ^{226}Ra. L'utilité de ^{226}Ra a été démontrée comme traceur et/ou comme chronomètre pour des processus magmatiques récents, pour la chronologie Holocène, pour des systèmes riverains et d'eau souterraine, et des études océanographiques (Ghaleb et al., 2004). Pour ces raisons, on a utilisé le ^{226}Ra pour déterminer la source de ces eaux et pour mieux comprendre la circulation du système et les effets de réinjection au niveau des puits.

L'analyse a été faite à l'Université du Québec à Montréal et est décrite dans l'article ci-joint. Les résultats se trouvent dans le tableau B.1.

Source	^{226}Ra (dpm/)	±
AZ2	0.9955	0.0184
AZ28	0.1688	0.0009
AZ33	3.0989	0.0215
Araro Nord	0.1189	0.0013
Bagnes 2	0.4022	0.0049
Chiflador	0.1141	0.0008
Currutaco	0.9955	0.0184

Tableau B.1. Teneur en ^{226}Ra (dpm/l) pour les puits et sources hydrothermales

En comparant ces résultats avec d'autres eaux thermales, on aperçoit qu'elles sont supérieures aux eaux thermales de Croatie et du basin Lodève mais sont inférieures à celles de la péninsule de Reykjanes (Tab. B.2).

Source	^{226}Ra (dpm/l)
Eaux thermales de Croatie*	0.00242 – 0.0734
Eaux du basin Lodève**	0.0374 – 0.0089
Eaux de la péninsule de Reykjanes***	6.01 – 26.46

Tableau B.2. Teneur en ^{226}Ra pour d'autres eaux thermales (* - Marović et al., 1996; ** - Condomines et al., 2010; *** - Kadko et al., 2007)

Comparées aux eaux thermales de Croatie et du basin Lodève, nos eaux sont enrichies en ^{226}Ra mais pas aussi riches que les eaux de la péninsule de Reykjanes. Les teneurs en ^{226}Ra de la péninsule de Reykjanes sont fortement marquées par une signature mantellique. Nos valeurs sont beaucoup plus faibles et on propose donc qu'elles possèdent une signature mantellique moins marquée. Il reste plusieurs analyses à faire sur des échantillons prélevés en janvier 2009 (puits : AZ9, AZ13, AZ13, AZ22, AZ51, AZ62; sources hydrothermales : Araro est, Araro ouest, Maritaro) avant que l'on puisse possiblement déterminer la source de ces eaux et comprendre la circulation du système hydraulique et les effets de réinjection. Ces résultats sont aussi discutés dans l'article ci-joint.

ANNEXE C

GAZ RARES

En 2008 et 2009, les gaz de 9 puits (AZ2, AZ9, AZ13, AZ17, AZ22, AZ28, AZ33, AZ51, et AZ62) et 9 sources hydrothermales (Araro Est, Araro Nord, Araro Ouest, Bagnes, Chiflador, Currutaco, Maritaro 1, Maritaro 2, et Tejamaniles) du champ géothermal Los Azufres ont été échantillonnés (Fig.A.1). Les gaz ont été analysés pour leurs teneurs en isotopes de gaz rares. La signature isotopique en gaz rares est un outil important pour déterminer l'histoire géologique et les processus géodynamiques majeurs de notre planète. Parmi les applications, les gaz rares dissous dans les eaux peuvent permettre de retracer l'origine de ces fluides et les interactions dans la croûte terrestre (e.g. Ballentine et al., 2002; Ozima et Podosek, 2002). Pour ces raisons, on utilise ces isotopes pour étudier le champ géothermale pour comprendre la circulation du champ, les effets de réinjection, et déterminer les sources du champ.

Pour échantillonner ces gaz, on utilise un tuyau en cuivre. Avant d'échantillonner, deux mâchoires sont attachées sur le tuyau: le premier est situé à environ un mètre du bout du tuyau et le deuxième environ 30 cm plus loin du premier (en s'éloignant du bout) (Fig.C.1).

Figure C.1. Échantillonnage des gaz rares au champ géothermale Los Azufres

Dans la plupart des cas, on répète cela pour être capable de prendre deux échantillons en même temps. Avant d'échantillonner, on ferme la mâchoire le plus loin du bout. Dans le cas d'un puits, on attache le bout aux tuyaux émettant des gaz des puits. Pour les sources, le bout est attaché à un entonnoir qui sera enfoncé dans la source. On laisse le gaz rentrer dans le tuyau pour quelques minutes. Après on ferme l'autre mâchoire et on coupe le tuyau à 5 cm de chaque vis. Cela nous donne notre échantillon de gaz qui est situé entre les deux vis.

Les échantillons ont été envoyés à l'Université de Michigan pour l'analyse des isotopes des gaz rares.

BIBLIOGRAPHIE GÉNÉRALE

Åberg. 1994. «The Use of Natural Strontium Isotopes as tracers in environmental studies, Water, Air and Soil Pollution». vol 79, no 1-4, p.309-322.

Anschutz, P., G. Blanc et P. Stille. 1995. «Origin of fluids and the evolution of the Atlantis II deep hydrothermal system, Red Sea: Strontium isotope study». Geochimica et Cosmochimica Acta. vol 59, no 23, p.4799-4808.

Appleby, P. G., et F. Oldfield. 1978. «The calculation of lead-210 dates assuming a constant rate of supply of unsupported 210Pb to the sediment». CATENA. no 5, p.1-8.

Appleby, P. G., P. J. Nolan, D. W. Gifford, M. J. Godfrey, F. Oldfield, N. J. Anderson et R. W. Battarbee. 1986. «210Pb dating by low background gamma counting, Hydrobiologia». vol 143, no 1, p.21-27.

Barrat, J.A., J. Boulègue, J.J. Tiercelin et M. Lesourd. 2000. «Strontium isotopes and rare-earth element geochemistry of hydrothermal carbonate deposits from Lake Tanganyika, East Africa». Geochimica et Cosmochimica Acta. vol 64, no 2, p.287-298.

Benes, P. et P. Strejc. 1986. «Interaction of radium with freshwater sediments and their mineral components». Journal of Radioanalytical and Nuclear Chemistry. vol 99, p.407-422.

Condomines M., C. Brouzes et S. Rhis. 1999. «Radium and its daughters in hydrothermal carbonates from Auvergne (French Massif Central): origin and dating applications». Comptes Rendus de l'Academie des Sciences Series IIA Earth and Planetary Science. vol 328, p. 23-28.

Condomines M., S. Rihs, E. Lloret et J.L. Seidel. 2010. «Determination of the four natural Ra isotopes in thermal waters by gamma-ray spectrometry». Applied Radiation and Isotopes. vol 68, p.384–391.

DePaolo, D.J. et B.L. Ingram. 1985. «High resolution stratigraphy with strontium isotopes». Science. vol 277, p. 938-941.

Ferrari, L., V.H. Garduño, G. Pasquarè et A. Tibaldi. 1991. «Geology of Los Azufres Caldera, Mexico, and its relationships with regional tectonics». Journal of Volcanology and Geothermal Research. vol 47, no 1-2, p. 129-148.

Ghaleb, B., E. Pons-Branchu et P. Deschamps. 2004. «Improved method for radium extraction from environmental samples and its analysis by thermal ionization mass spectrometry». Journal of Analytical Atomic Spectrometry. vol 19, p.906-910.

González-Partida, E., A. Carrillo-Chávez, G. Levresse, E. Tello-Hinojosa, S. Venegas-Salgado, G. Ramirez-Silva, M. Pal-Verma, J. Tritlla, et A. Camprubi. 2005. «Hydro-geochemical and isotopic fluid evolution of the Los Azufres geothermal field, Central Mexico». Applied Geochemistry. vol 20, p. 23-39.

Herndon, J.M. 2003. «Nuclear georeactor origin of oceanic basalt ^{3}He/^{4}He evidence, and implications». PNAS. vol 100, no 6, p.3047-3050.

Hoke, L., D.R. Hilton, S.H. Lamb, K. Hammerschmidt, et H. Friedrichsen. 1994. «^{3}He evidence for a wide zone of active mantle melting beneath the Central Andes». Earth and Planetary Science Letters. vol 128, no 3-4, p.341-355.

Johnson, R.W. et R.J. Arculus. 1978. «Volcanic rocks of the Witu islands, Papua New Guinea: the origin of magmas above the deepest part of the New Britain Benioff Zone». Bulletin of Volcanology. vol 41, no 4, p.609-655.

Ozima, M. et F.Podosek. 2002. *Nobel Gas Geochemistry*. United States of America: Cambridge University Press, 2nd Edition, p.1-5.

Rihs, S., M. Condomines et Ch. Fouillac. 1997. «U- and Th-series radionuclides in CO2-rich geothermal systems in the French Massif Central». Journal of Radioanalytical and Nuclear Chemistry. vol 226, p.149-157.

Rihs, S. et M. Condomines. 2002. «An improved method for Ra isotope (226Ra, 228Ra, 224Ra) measurements by gamma spectrometry in natural waters: application to CO2-rich thermal waters from the French Massif Central». Chemical Geology. vol 182, p.409-421.

Segovia, N., R.M. Barragan, E. Tello, R. Alfaro et M. Mena. 2005. «Geochemical Characteristics and ^{222}Rn Measurements at Cuitzeo Basin (Mexico) Thermal Springs and Artesian Wells». Proceedings World Geothermal Congress. Antalya, Turkey, p.1-6.